Electronic Supplementary Material (ESI) for New Journal of Chemistry.

Supporting Information

π-Extended indoloquinoxaline functionalized triarylamines with ethynyl and tetracyanobutadiene bridges for p-channel and ambipolar OFETs

Paneerselvam Devibala,[‡] Balu Balambiga,[‡] Predhanekar M. Imran,[§] and Samuthira Nagarajan[‡]*

[‡] Department of Chemistry, Central University of Tamil Nadu, Thiruvarur- 610 005, India
[§] Department of Chemistry, Islamiah College, Vaniyambadi - 635 752, India

1. GENERAL INFORMATION

Triphenylamine, 5-bromoisatin, 1-bromohexane, o-phenylenediamine, tetracyanoethylene, 4-tert-butylphenylboronic acid, $Pd(PPh_3)_2Cl_2$, $Pd(PPh_3)_4$, $Pd(dppf)Cl_2$, Bis(pinacolato)diborane, copper iodide, dioxane, trimethylsilylacetyelene, N-bromosuccinamide (NBS), $POCl_3$, potassium iodide, potassium iodate, sodium carbonate, potassium tert-butoxide, and acetic acid were used as received from the commercial sources. Anhydrous dimethylformamide (DMF), tetrahydrofuran (THF), and triethylamine solvents were used as received. ACS-grade solvents were used for spectroscopic analysis.
^1H and ^{13}C NMR spectra were recorded in Bruker 400 MHz spectrometer using tetramethylsilane (TMS) as internal standard and $CDCl_3$ as solvent. High-resolution mass spectra were obtained from Thermo Exactive Plus UHPLC-MS. Absorption and emission spectra were recorded using a JASCO UV-NIR spectrophotometer and Perkin-Elmer LS 55 spectrophotometer, respectively. Electrochemical studies were performed in CHI electrochemical workstation (CHI 6035D). A conventional three-electrode cell setup was used in an anhydrous dichloromethane solvent with tetrabutylammonium hexafluorophosphate (TBAPF6) as a supporting electrolyte. Thermal studies were carried out in TA thermal analyzer. OFET characterizations were carried out using Keithley 4200A semiconductor parameter analyzer at ambient conditions.

2. SYNTHESIS OF COMPOUNDS 1-10

Compound 1: 5-Bromoisatin (1.0 g, 4.42 mmol) in DMF and potassium carbonate (1.22 g, 8.8 mmol) was stirred at 0˚C for 1 hour. Bromohexane (0.73 g, 4.42 mmol) was added to the reaction mixture and stirred at room temperature for 12 hours. The resultant mixture was poured over water and extracted with dichloromethane. The combined organic phase was dried over anhydrous Na_2SO_4, and the solvent was removed under reduced pressure. The crude was purified by column chromatography on silica gel (EtOAc: n-hexane) to afford compound **1** as red crystals. ^1H NMR (400 MHz, $CDCl_3$) δ 7.73 – 7.67 (m, 2H), 6.81 (d, *J* = 7.9 Hz, 1H), 3.74 – 3.68 (m, 2H), 1.71-1.64 (m, 2H), 1.38-1.30 (m, 7.6 Hz, 6H), 0.89 (t, *J* = 7.0 Hz, 3H). ^{13}C NMR (100 MHz, $CDCl_3$) δ 182.5, 157.4, 149.8,140.5, 128.3, 118.8, 116.4, 111.8, 40.4, 31.3, 27.1, 26.5, 22.5, 13.9.

Compound 2: A mixture of compound **1** (1.0 g, 3.23 mmol) and o-phenylenediamine (0.35 g, 3.23 mmol) was dissolved in acetic acid and refluxed for 3 hours. The resultant mixture was poured over ice water and extracted with dichloromethane. The combined organic phase was dried over anhydrous Na_2SO_4, and the solvent was removed under reduced pressure. The crude was purified by column chromatography on silica gel (EtOAc: n-hexane) to afford compound **2.** ^1H NMR (400 MHz, $CDCl_3$) δ 8.60 (s, 1H), 8.28 (d, *J* = 8.0 Hz 1H), 8.14 (d, *J* = 8.4 Hz, 1H), 7.79-7.75(m, 2H), 7.69 (t, *J* = 7.4 Hz, 1H), 7.36 (d, *J* = 8.6 Hz, 1H), 4.46 (t, *J* = 7.0 Hz, 2H), 1.97 – 1.87 (m, 2H), 1.45 – 1.23 (m, 6H), 0.86 (t, *J* = 7.2 Hz, 3H). ^{13}C NMR (100 MHz, $CDCl_3$) δ 145.5, 142.9, 140.9, 139.4, 138.7, 133.4, 129.4, 129.2, 127.8, 126.2, 125.4, 121.0, 113.5, 111.0, 41.6, 31.4, 28.4, 26.7, 22.5, 14.0.

Compound 3: Compound **2** (1 g, 2.62 mmol) in dioxane (10 mL) was taken under a nitrogen atmosphere to which $PdCl_2$(dppf) (0.097g, 0.05 mol %) and potassium acetate (0.38 g, 3.93 mmol) were added. Bis(pinacolato)diborane (0.66 g, 2.62 mmol) was introduced after 20 minutes, and the mixture was refluxed for 24 hours. After being washed with brine solution, the organic phase was separated using dichloromethane, and the solvent was removed under reduced pressure to afford **3** as a yellow solid. ^1H NMR (400 MHz, $CDCl_3$) δ 9.02 (s, 1H), 8.30 (d, *J* = 8.3 Hz, 1H), 8.13 (t, *J* = 7.8 Hz, 2H), 7.80 – 7.73 (m, 1H), 7.68 (t, *J* = 7.6 Hz, 1H), 7.47 (d, *J* = 8.2 Hz, 1H), 4.49 (t, *J* = 7.3 Hz, 2H), 2.00 – 1.89 (m, 2H), 1.39 (s, 12H), 1.36-1.23 (m, 6H), 0.86 (t, *J* = 7.2 Hz, 3H). ^{13}C NMR (100 MHz, CDCl3) δ 146.5, 145.8, 140.6, 140.2, 139.5, 137.1, 130.1, 129.4, 128.6, 127.8, 125.9, 119.1, 108.8, 83.8, 41.5, 31.4, 28.4, 26.7, 24.9, 22.5, 14.0.

Compound 4: In a two-necked round-bottomed flask, compound **2** (1 g, 2.62 mmol) in a 1:2 mixture of dry THF (10 mL) and Et_3N (20 mL) was taken under a nitrogen atmosphere, followed by $PdCl_2(PPh_3)_2$ (0.09 g, 0.05 mol %) and CuI (0.25 g, 0.05 mol %) were added. Ethynyldimethylsilanol (0.35 g, 3.40 mmol) was introduced after 10 minutes, and the mixture was refluxed for 24 hours. After being washed with brine solution, the organic phase was separated using dichloromethane and evaporated under reduced pressure to afford 0.72 g (67 %) of ((6-hexyl-6H-indolo[2,3-b]quinoxalin-9-yl)ethynyl)dimethylsilanol as a yellow solid. The obtained ((6-hexyl-6H-indolo[2,3-b]quinoxalin-9-yl)ethynyl)dimethylsilanol (0.72 g, 1.79 mmol) and KOH (0.1 g, 1.79 mmol) was dissolved in toluene and refluxed for 5 hours. The reaction mixture was poured over water and extracted with dichloromethane. The crude product was purified by column chromatography on silica gel (EtOAc: n-hexane) to afford 0.55 g (94 %) of

compound **4** as a yellow powder. ^{1}H NMR (400 MHz, $CDCl_3$) δ 8.63 (s, 1H), 8.30 (d, *J* = 9.7 Hz, 1H), 8.14 (d, *J* = 8.4 Hz, 1H), 7.81-7.75 (m, 2H), 7.69 (t, *J* = 7.6 Hz, 1H), 7.42 (d, *J* = 8.4 Hz, 1H), 4.48 (t, *J* = 7.3 Hz, 2H), 3.13 (s, 1H), 2.01 – 1.87 (m, 2H), 1.45 – 1.22 (m, 6H), 0.86 (t, *J* = 7.2 Hz, 3H). ^{13}C NMR (100 MHz, $CDCl_3$) δ 145.8, 144.1, 140.7, 139.4, 139.3, 134.5, 129.4, 129.0, 127.9, 126.7, 126.2, 119.4, 114.3, 109.5, 83.7, 76.4, 41.6, 31.4, 28.4, 26.7, 22.5, 14.0.

9-Ethynyl-6-hexyl-6H-indolo[2,3-b] quinoxaline, 4:

General procedure for compounds 8a-b: In a two-necked round-bottomed flask, compound **5** or **8** (1 mmol) in dry THF (10 mL) was taken under a nitrogen atmosphere, followed by $Pd(PPh_3)_4$ (0.05 mol %) and sodium carbonate (5 mL of 2M aqueous solution) were added. The resultant mixture was stirred for 20 minutes at room temperature. Then compound **3** (1 mmol) was introduced, and the mixture refluxed for 5-24 hours, respectively. After being washed with brine solution, the organic phase was separated using dichloromethane and removed under reduced pressure. The crude product was purified by column chromatography on silica gel (EtOAc: n-hexane) to afford compound **8a-b.**

Compound 8a: Yellow powder (0.39 g, 71%). ^{1}H NMR (400 MHz, $CDCl_3$) δ 8.67 (s, 1H), 8.28 (d, *J* = 8.3 Hz, 1H), 8.12 (d, *J* = 8.4 Hz, 1H), 7.86 (d, *J* = 8.4 Hz, 1H), 7.73 (t, *J* = 8.4 Hz, 1H), 7.64 (t, *J* = 8.0 Hz, 1H), 7.59 (d, *J* = 8.0 Hz, 2H), 7.43 (d, *J* = 8.4 Hz, 1H), 7.27 (t, *J* = 8.4 Hz, 4H), 7.16 (t, *J* = 8.3 Hz, 6H), 7.03 (t, *J* = 7.3 Hz, 2H), 4.43 (t, *J* = 7.3 Hz, 2H), 1.97 – 1.89 (m, 2H), 1.43 -1.25 (m, 6H), 0.85 (t, *J* = 7.2 Hz, 3H). ^{13}C NMR (100 MHz, $CDCl_3$) δ 147.7, 146.9, 145.9, 143.4, 140.7, 140.1, 139.2, 134.8, 133.7, 129.6, 129.3, 129.3, 128.7, 127.8, 127.7, 125.9, 124.4, 124.1, 122.9, 120.4, 119.9, 109.7, 41.5, 31.5, 28.5, 26.7, 22.6, 14.0. HRMS (ESI) (m/z) 547.2858 [M+H]; Calculated for $C_{38}H_{34}N_4$: 547.2817.

Compound, 8b: Yellow-orange powder (0.55 g, 68 %) ^{1}H NMR (400 MHz, $CDCl_3$) δ 8.74 (s, 1H), 8.32 (d, *J* = 8.3 Hz, 1H), 8.15 (d, *J* = 8.4 Hz, 1H), 7.96 (d, *J* = 8.5 Hz, 1H), 7.77 (t, *J* = 4.9 Hz, 1H), 7.67 (d, *J* = 8.4 Hz, 2H), 7.56-7.52 (m, 10H), 7.47 (d, *J* = 8.1 Hz, 4H), 7.30-7.24 (m, 6H), 4.52 (t, *J* = 7.2 Hz, 2H), 2.02 – 1.95 (m, 2H), 1.72-1.70 (m, 2H), 1.37 (s, 18H), 1.36 – 1.24 (m, 4H), 0.88 (t, *J* = 7.0 Hz, 3H). ^{13}C NMR (100 MHz, $CDCl_3$) δ 149.8, 146.7, 146.6, 146.0, 143.4, 140.7, 140.1, 139.2, 137.7, 135.5, 135.1, 133.7, 129.7, 129.3 128.7, 127.8, 127.8, 127.7, 126.3, 125.9, 125.6, 124.5, 124.4, 120.5, 120.0, 109.8, 41.6, 34.5, 31.5, 31.4, 28.5, 26.7, 22.5, 14.0. HRMS (ESI) (m/z) 811.4712 [M+H]; Calculated for $C_{58}H_{58}N_4$: 811.4695.

General procedure for compounds 9a-b: In a 100 mL round-bottomed flask, a mixture of compound **5** or **8** (1 mmol), $PdCl_2(PPh_3)_2$ (0.05 mol %), and CuI (0.05 mol%) was dissolved in 1:1 mixture of dry THF (10mL) and Et_3N (10mL) under N_2. Compound **4** (1 mmol) was added to the mixture and refluxed at 70 ^{o}C for 12 hours. After being washed with brine solution, the organic phase was separated using dichloromethane, and the solvent was removed under reduced pressure. The crude was purified by column chromatography on silica gel (DCM: n-hexane) to afford compounds **9a** and **9b,** respectively.

Compound 9a: Yellow powder (0.45 g, 79 %) ^{1}H NMR (400 MHz, $CDCl_3$) δ 8.64 (s, 1H), 8.30 (d, *J* =8.2 Hz, 1H), 8.14 (d, *J* = 8.6 Hz, 1H), 7.82 (d, *J* = 8.4 Hz, 1H), 7.77 (t, *J* = 7.8 Hz, 1H), 7.69 (t, *J* = 8.0 Hz, 1H), 7.49 – 7.35 (m, 4H), 7.28 (t, *J* = 8.0 Hz, 4H), 7.13 (d, *J* = 7.7 Hz, 3H), 7.08-7.00 (m, 4H), 4.49 (t, *J* = 7.3 Hz, 2H), 2.02 – 1.90 (m, 2H), 1.43 – 1.27 (m, 6H), 0.87 (t, *J* = 7.1 Hz, 3H). ^{13}C NMR (100 MHz, $CDCl_3$) δ 147.8, 147.8, 147.2, 145.9, 143.6, 140.7, 139.5, 139.4, 133.9, 132.4, 129.4, 29.4, 128.9, 127.8, 126.1, 125.9, 124.9, 123.5, 122.4, 119.6, 116.3, 116.0, 109.5, 88.9, 88.7, 41.6, 31.4, 28.4, 26.7, 22.5, 14.0. HRMS (ESI) (m/z) 571.2870 [M+H]; Calculated for $C_{40}H_{34}N_4$: 571.2817.

Compound 9b: Yellow powder (0.6 g, 72 %) ^{1}H NMR (400 MHz, $CDCl_3$) δ 8.57 (s, 1H), 8.22 (d, *J* = 8.3 Hz, 1H), 8.05 (d, *J* = 8.4 Hz, 1H), 7.74 (d, *J* = 8.4 Hz, 1H), 7.67 (d, *J* = 8.4 Hz, 1H), 7.60 (t, *J* = 7.0 Hz, 1H), 7.46-7.43 (m, 8H), 7.39-7.36 (m, 6H), 7.35 (d, *J* = 8.6 Hz, 1H), 7.13 (d, *J* = 8.6 Hz, 4H), 7.06 (d, *J* = 8.7 Hz, 2H), 4.39 (t, *J* = 7.3 Hz, 2H), 1.91 – 1.83 (m, 2H), 1.63-1.61 (m, 2H), 1.28 (s, 18H), 1.27-1.17 (m, 4H), 0.79 (t, *J* = 7.2 Hz, 3H). ^{13}C NMR (100 MHz, $CDCl_3$) δ 149.9, 147.5, 146.1, 145.9, 143.6, 140.7, 139.5, 139.4, 137.6, 136.0, 134.0, 132.5, 129.4, 128.9, 127.8, 126.5, 126.4, 126.1, 125.9, 125.7, 124.9, 122.9, 119.6, 116.7, 116.0, 109.5, 89.0, 88.8, 41.6, 34.5, 31.4, 31.4, 28.5, 26.7, 22.5, 14.0. HRMS (ESI) (m/z) 835.4691 [M+H]; Calculated for $C_{60}H_{58}N_4$: 835.4695.

General procedure for compounds 10a-b: In a 100 mL round-bottomed flask, compound **9a** or **9b** was dissolved in dichloromethane under dark conditions. Then tetracyanoquinodimethane (1 mmol) was added, and the resultant

mixture was stirred for 5 mins at room temperature. The solvent was removed under reduced pressure, and the crude was purified by column chromatography on silica gel (DCM: n-hexane) to afford compounds **10a** and **10b,** respectively.

Compound, 10a: Dark-red solid (0.66g, 95%) ^{1}H NMR (400 MHz, $CDCl_3$) δ 8.57 (s, 1H), 8.31 (d, *J* = 8.8, 1H), 8.24 (d, *J* = 7.2 Hz, 1H), 8.11 (d, *J* = 8 Hz, 1H), 7.77 (t, *J* = 8.4 Hz, 1H), 7.69 (d, *J* = 8.1 Hz, 3H), 7.58 (d, *J* = 8.8 Hz, 1H), 7.32 (t, *J* = 7.8 Hz, 4H), 7.19 – 7.13 (m, 6H), 6.88 (d, *J* = 9.2 Hz, 2H), 4.47 (t, *J* = 7.4 Hz, 2H), 1.95 – 1.86 (m, 2H), 1.38 – 1.30 (m, 4H), 1.26-1.23 (m, 2H), 0.81 (s, 3H). ^{13}C NMR (100 MHz, $CDCl_3$) δ 168.1, 164.4, 153.9, 147.4, 146.0, 144.5, 141.0, 139.9, 138.5, 132.1, 131.6, 130.1, 129.9, 129.4, 128.3, 127.4, 126.9, 126.7, 125.1, 124.2, 121.9, 120.7, 118.2, 113.7, 113.0, 112.9, 111.9, 110.9, 83.6, 78.2, 42.1, 31.3, 28.5, 26.7, 22.5, 14.0. HRMS (ESI) (m/z) 698.2917 [M+H]; Calculated for $C_{46}H_{34}N_8$: 698.2906.

Compound, 10b: Dark-red solid (0.92 g, 95%)^{1}H NMR (400 MHz, $CDCl_3$) δ 8.59 (s, 1H), 8.33 (d, *J* = 8.8 Hz, 1H), 8.25 (d, *J* = 8.3 Hz, 1H), 8.12 (d, *J* = 8.4 Hz, 1H), 7.79-7.76 (m, 4H), 7.59 (d, *J* = 8.4 Hz, 1H), 7.54 (d, *J* = 8.4 Hz, 4H), 7.46-7.29 (m, 8H), 7.25 (d, *J* = 8.5 Hz, 4H), 7.01 (d, *J* = 9.2 Hz, 2H), 4.47 (t, *J* = 7.3 Hz, 2H), 1.95 – 1.87 (m, 2H), 1.39-1.34 (m, 2H), 1.29 (s, 18H), 1.24 – 1.20 (m, 4H), 0.81 (s, 3H). ^{13}C NMR (100 MHz, $CDCl_3$) δ 167.9, 164.2, 153.6, 150.7, 147.5, 147.5, 146.1, 143.3, 141.0, 139.9, 139.4, 138.6, 137.0, 132.2, 131.8, 129.9, 129.5, 128.5, 128.3, 127.2, 127.0, 126.6, 125.8, 125.1, 124.2, 122.2, 120.7, 118.5, 114.2, 113.3, 110.8, 83.6, 78.2, 42.1, 36.6, 34.5, 34.5, 31.3, 28.5, 26.7, 22.5, 14.0. HRMS (ESI) (m/z) 962.4784 [M+H]; Calculated for $C_{66}H_{58}N_8$: 962.4796.

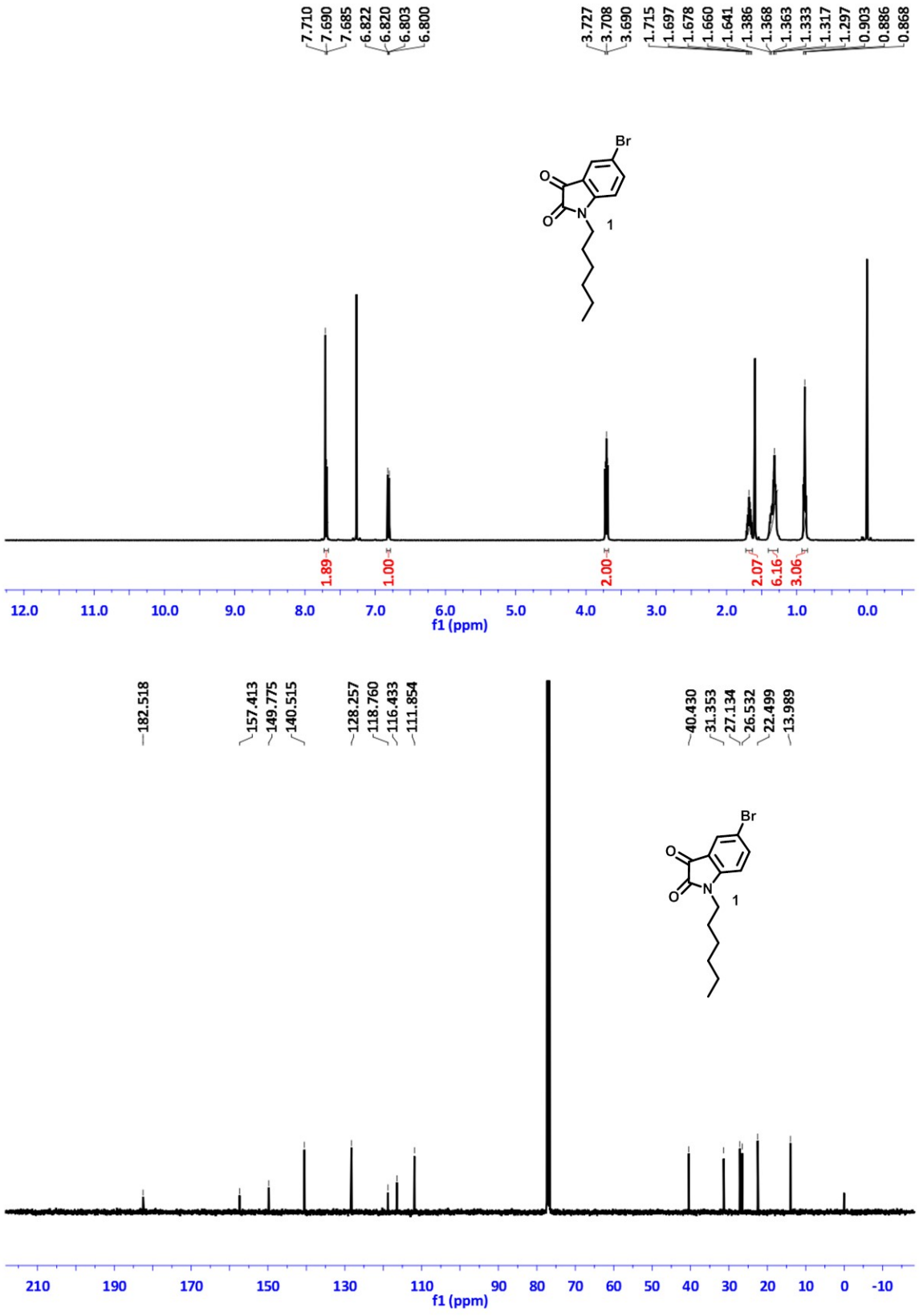

Figure S1: ^{1}H and ^{13}C NMR spectra of compound 1

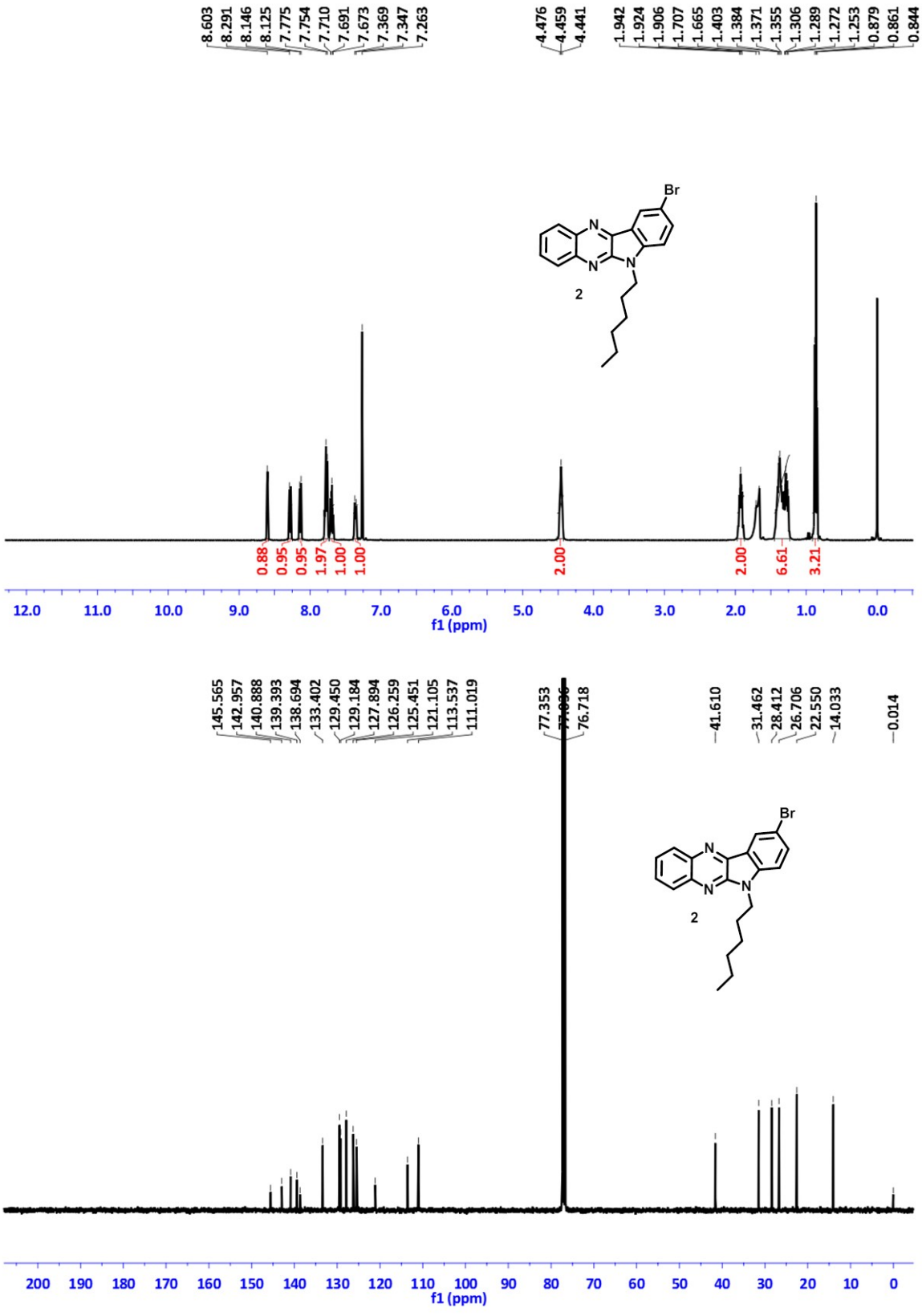

Figure S2: ^{1}H and ^{13}C NMR spectra of compound 2

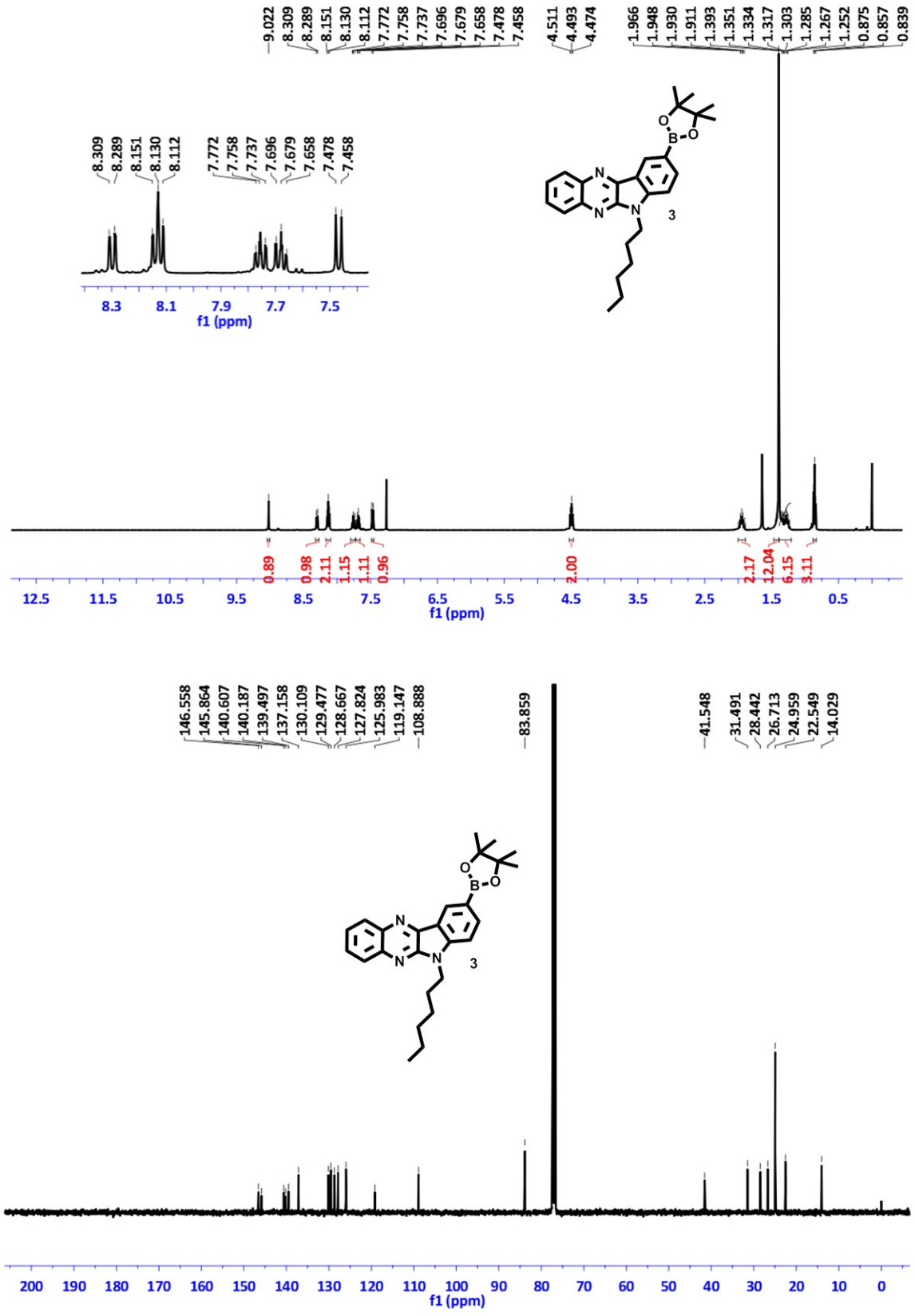

Figure S3: ^{1}H and ^{13}C NMR spectra of compound 3

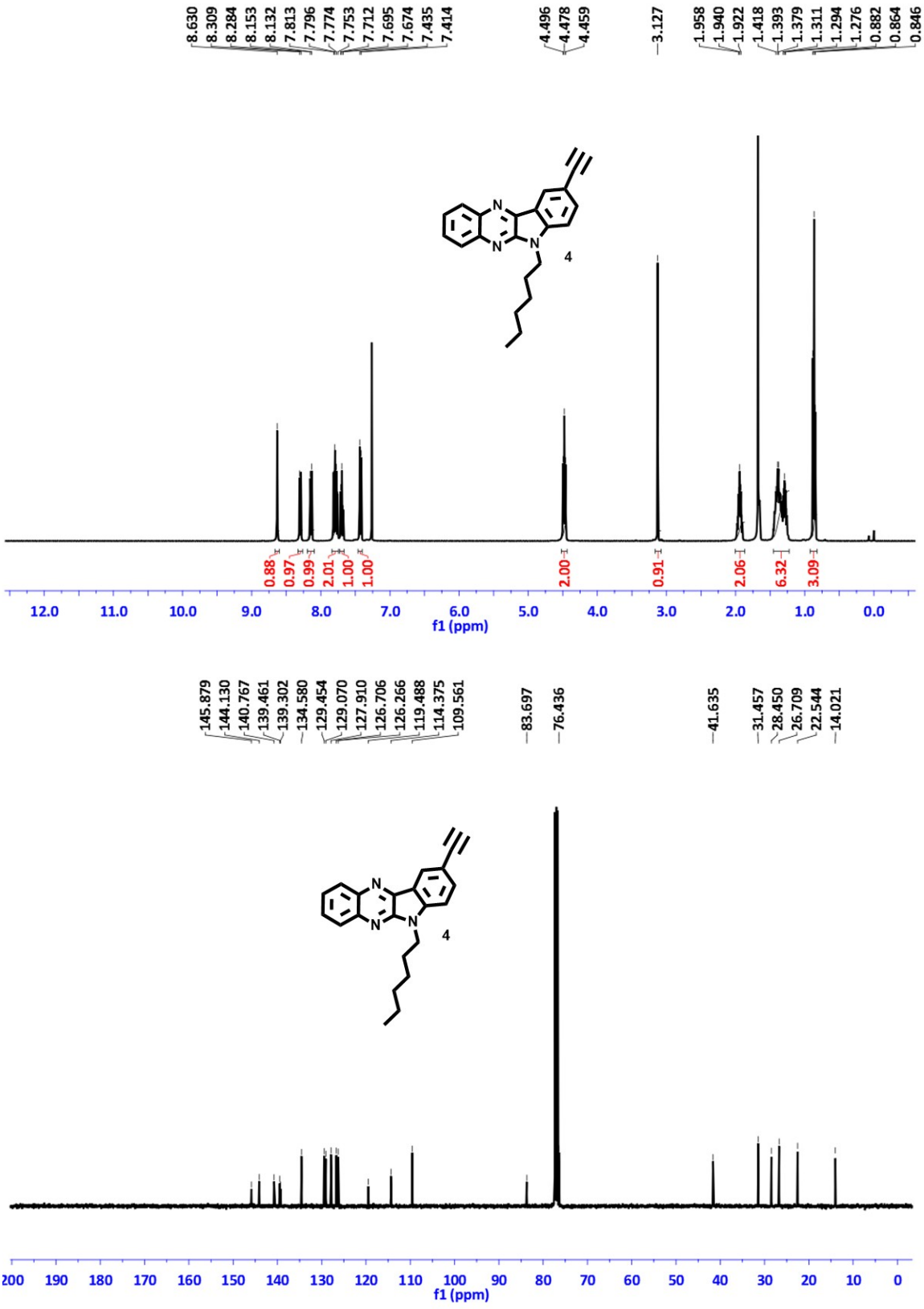

Figure S4: ^{1}H and ^{13}C NMR spectra of compound 4

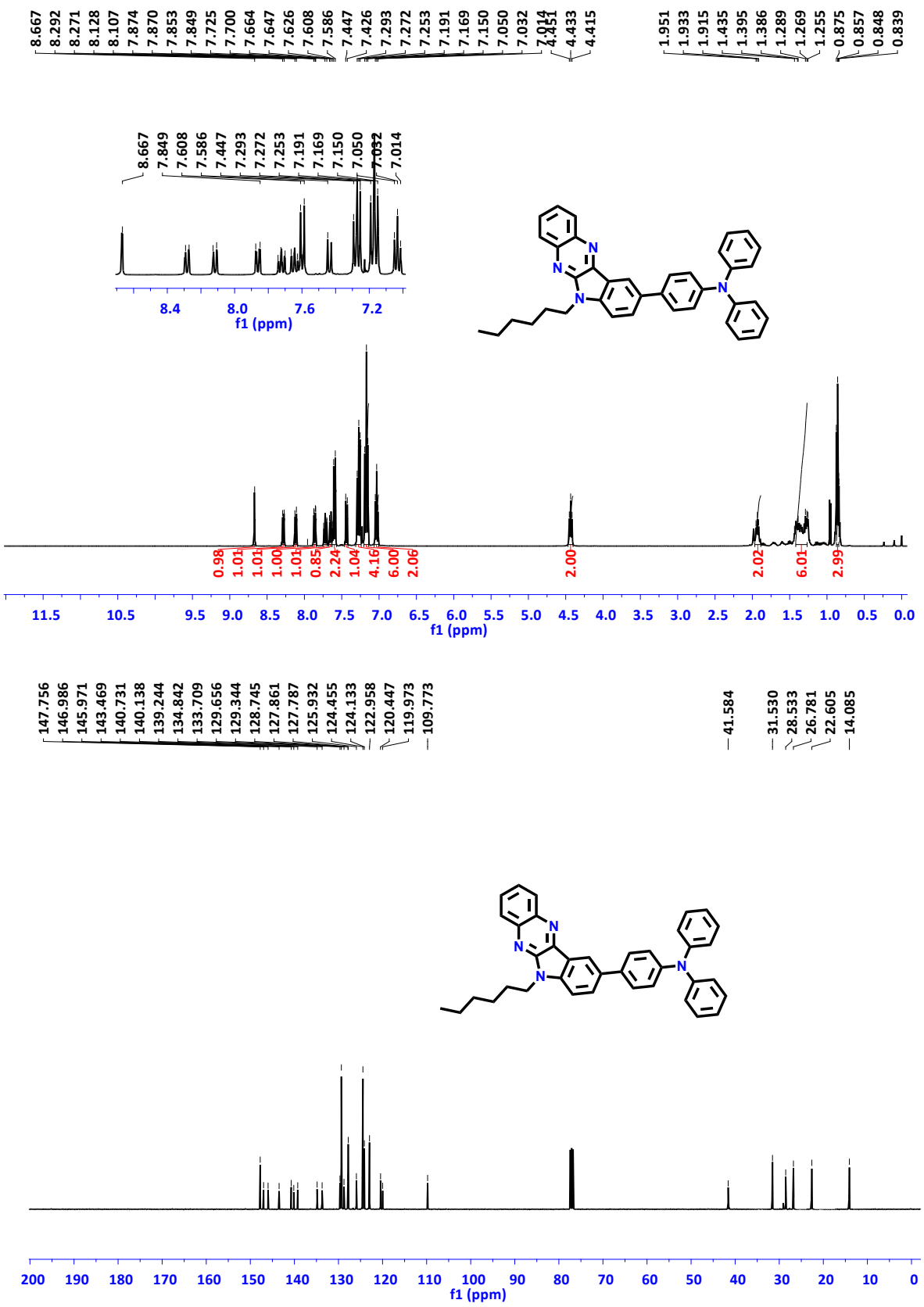

Figure S5: ^{1}H and ^{13}C NMR spectra of compound 8a

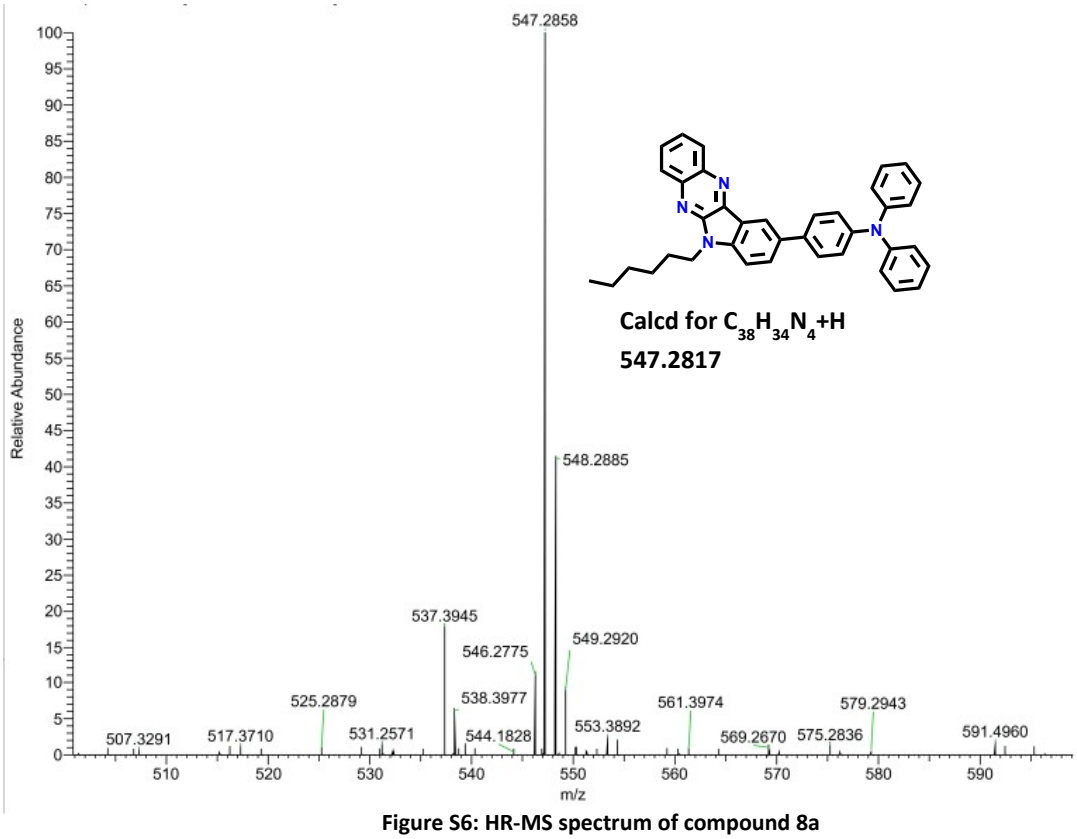

Figure S6: HR-MS spectrum of compound 8a

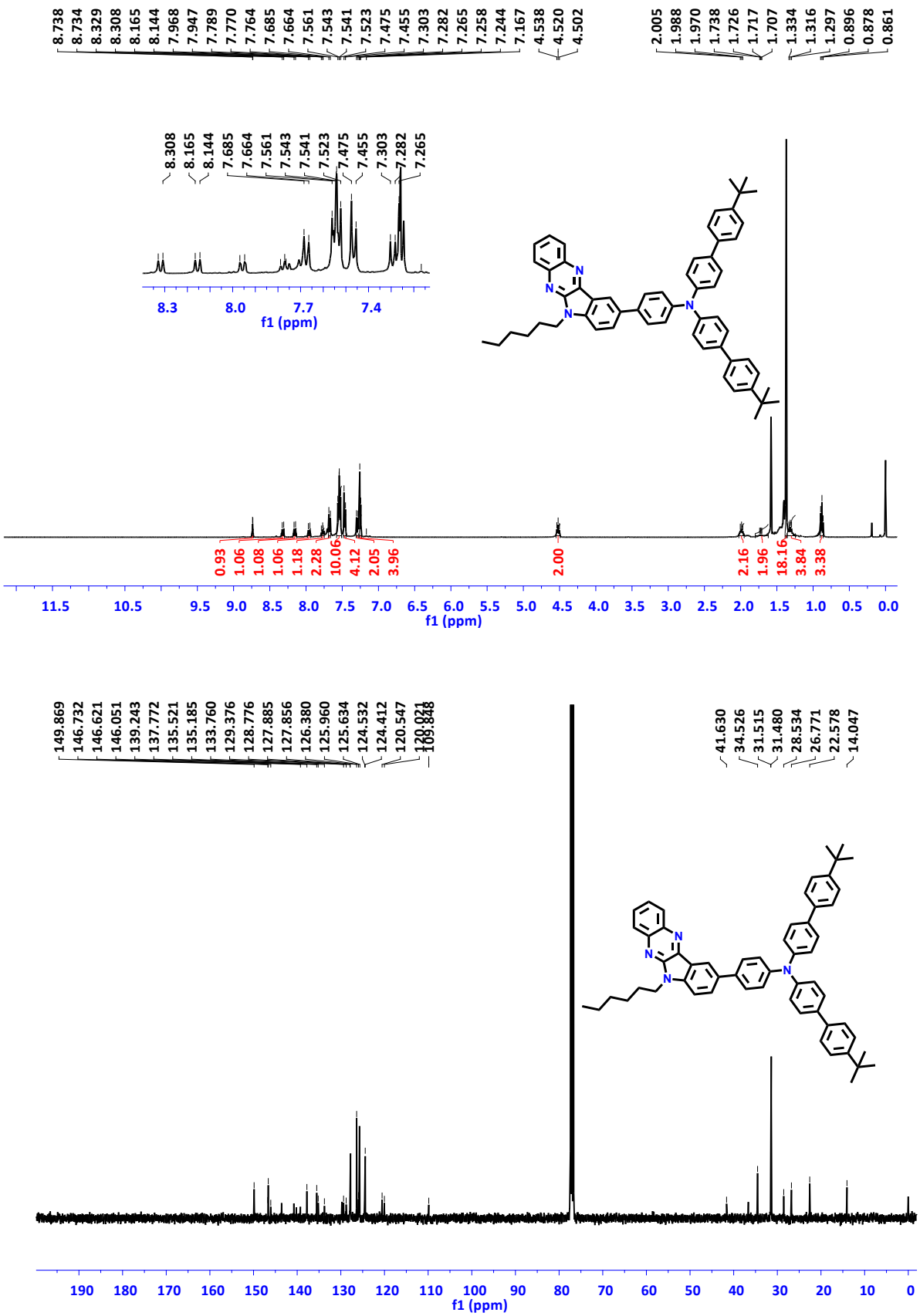

Figure S7: ^{1}H and ^{13}C NMR spectra of compound 8b

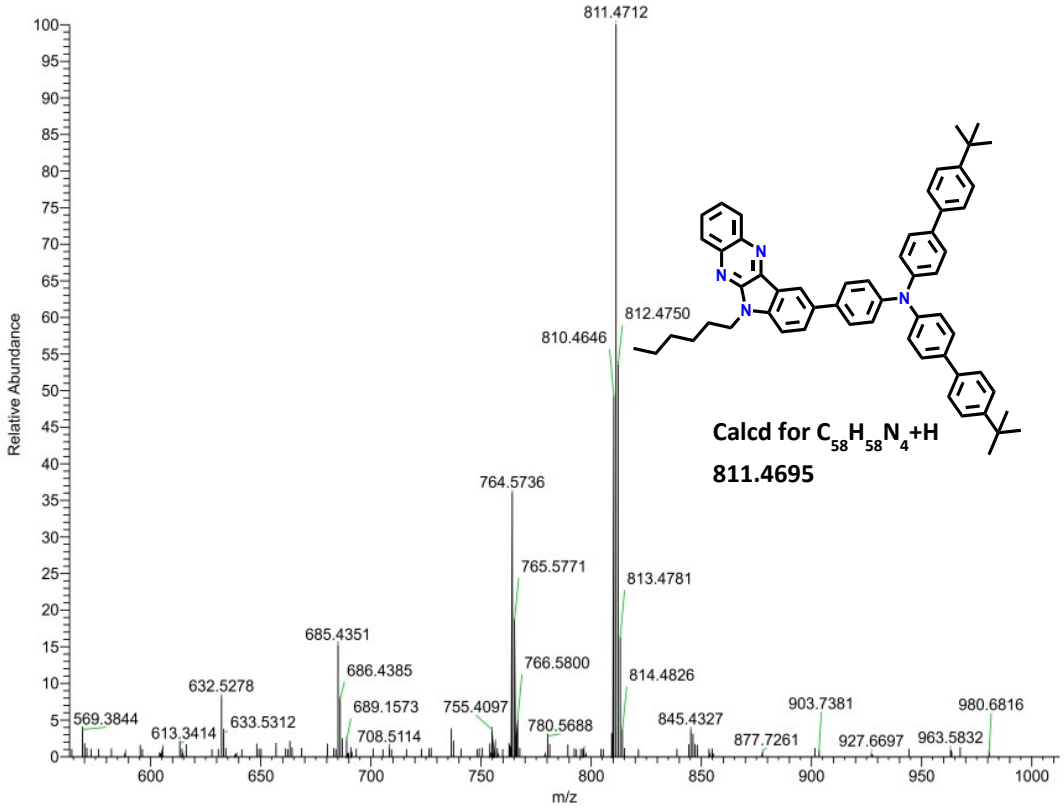

Figure S8: HR-MS spectrum of compound 8b

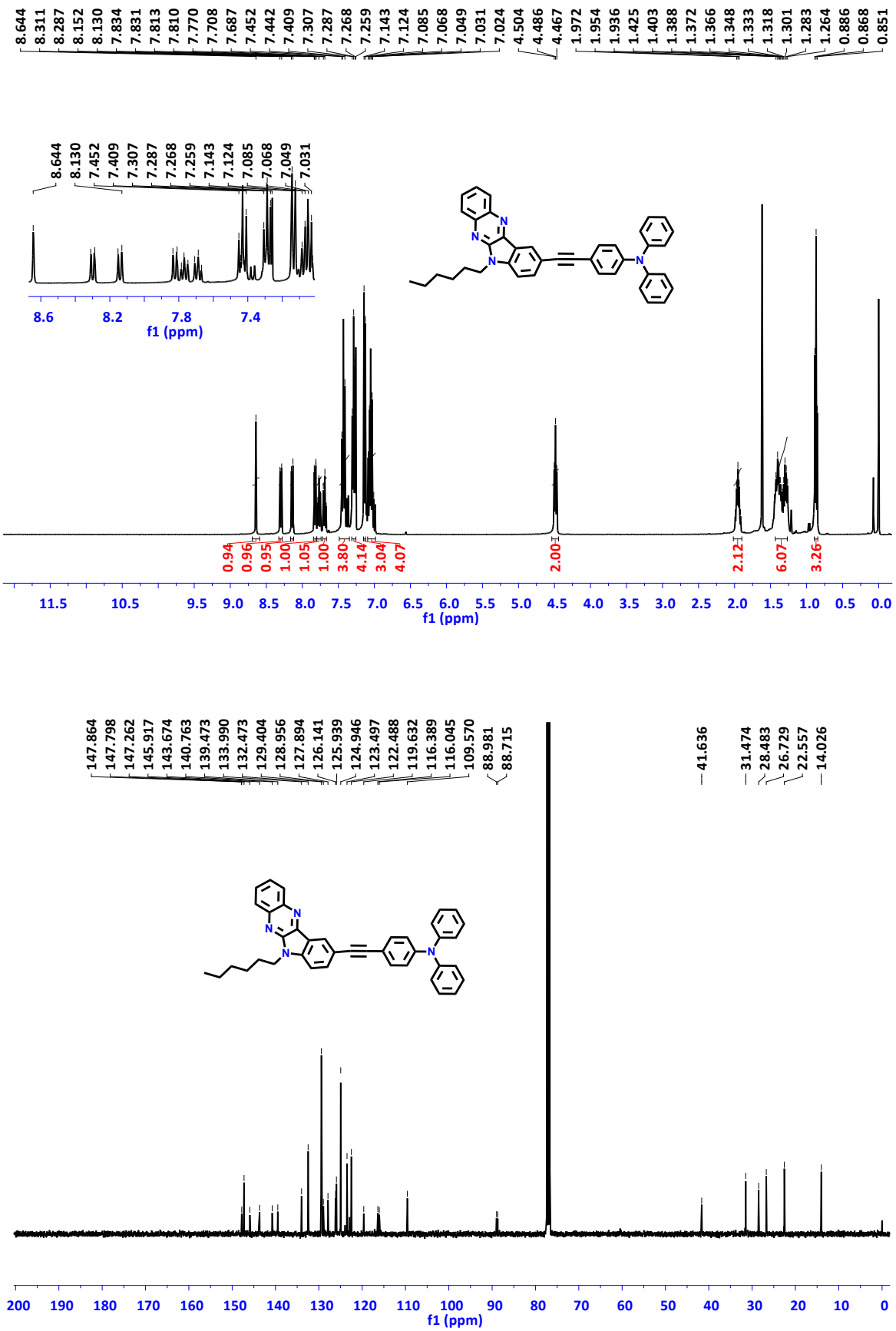

Figure S9: ^{1}H and ^{13}C NMR spectra of compound 9a

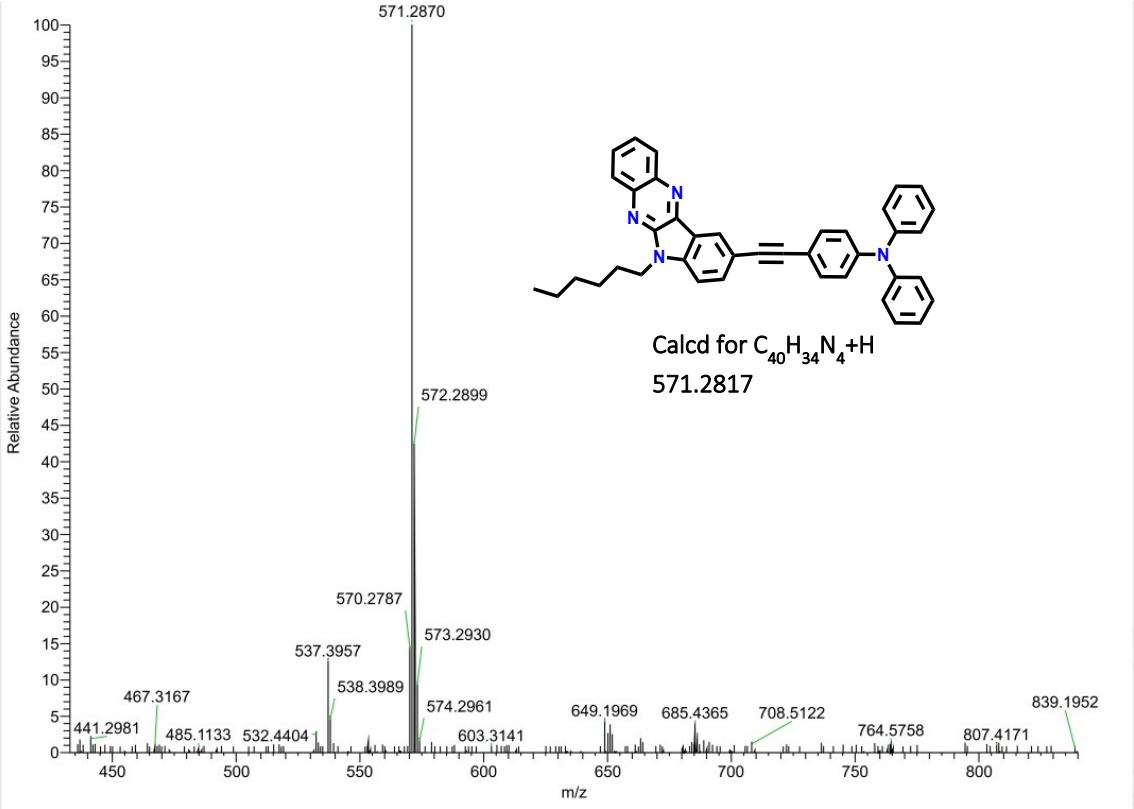

Figure S10: HR-MS spectrum of compound 9a

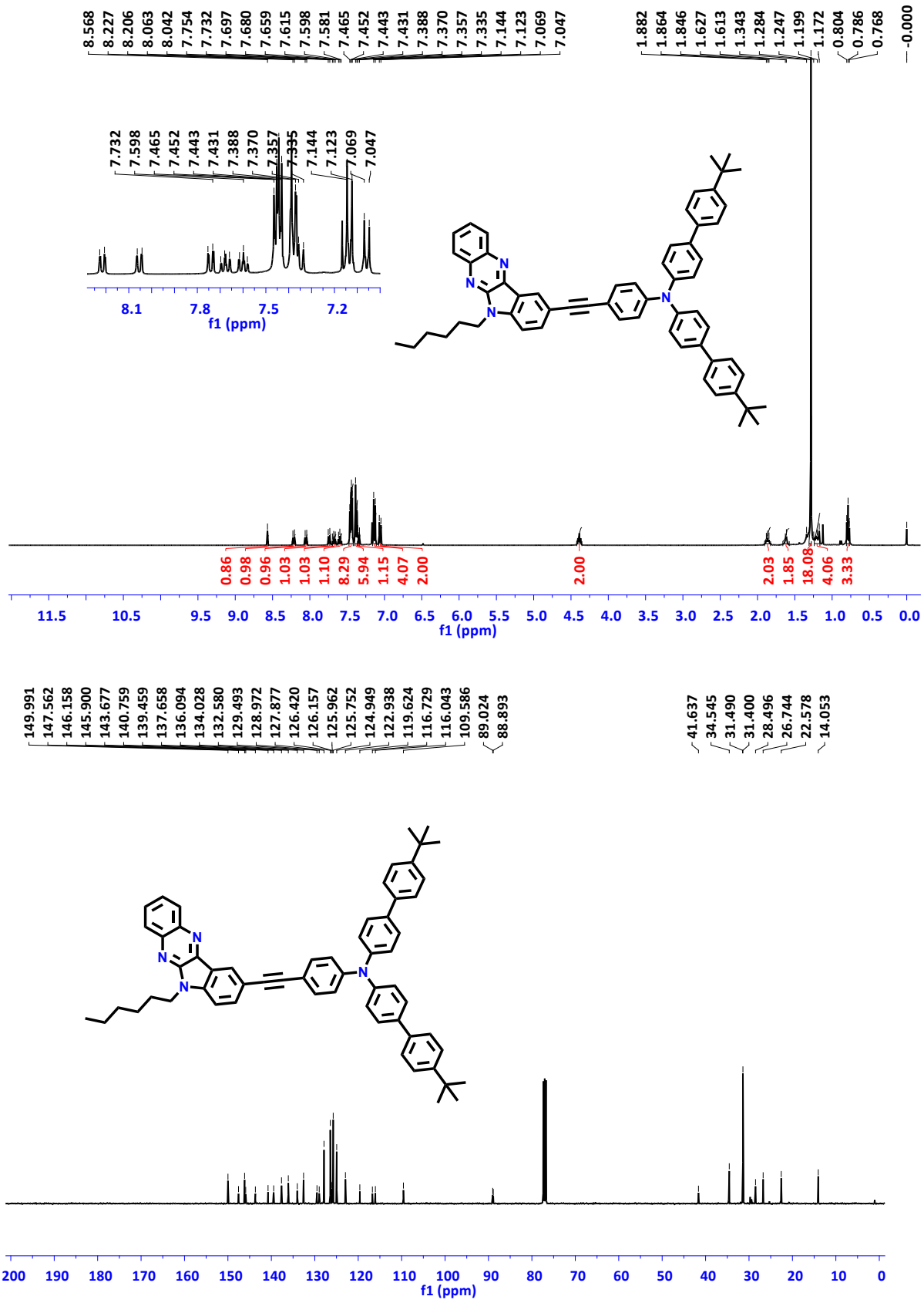

Figure S11: ^{1}H and ^{13}C NMR spectra of compound 9b

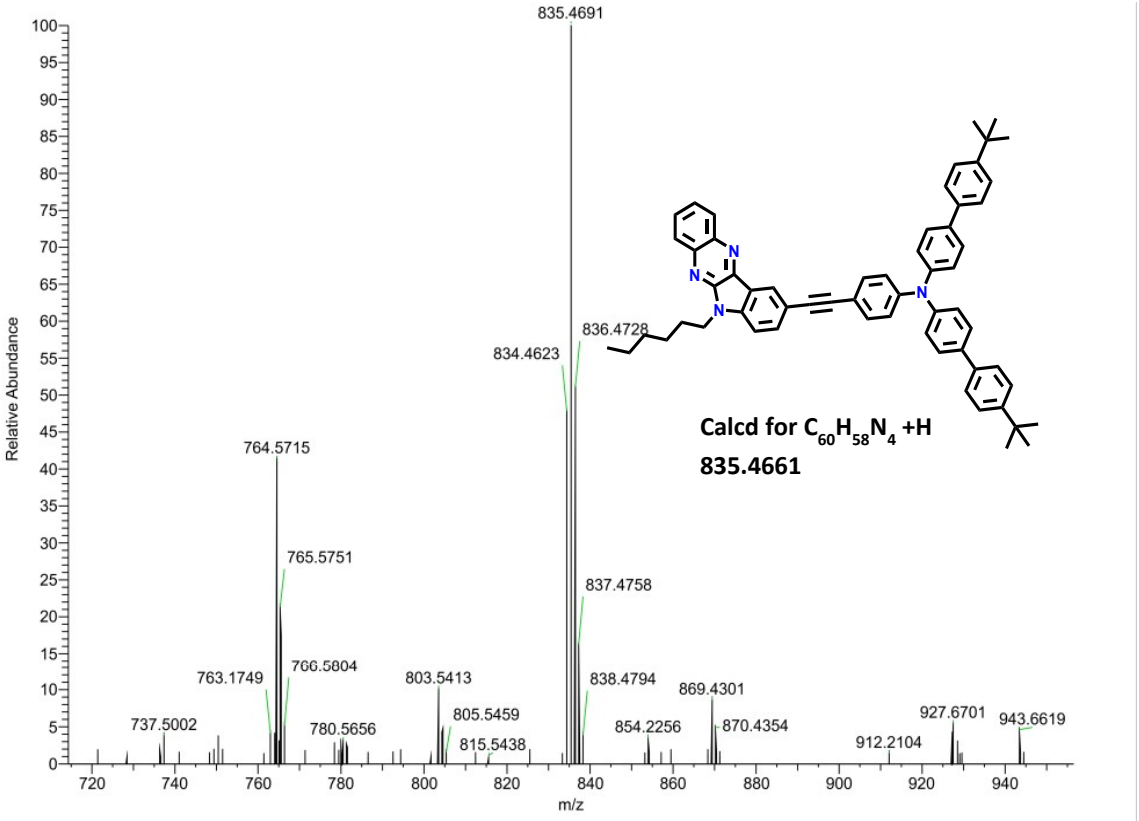

Figure S12: HR-MS spectrum of compound 9b

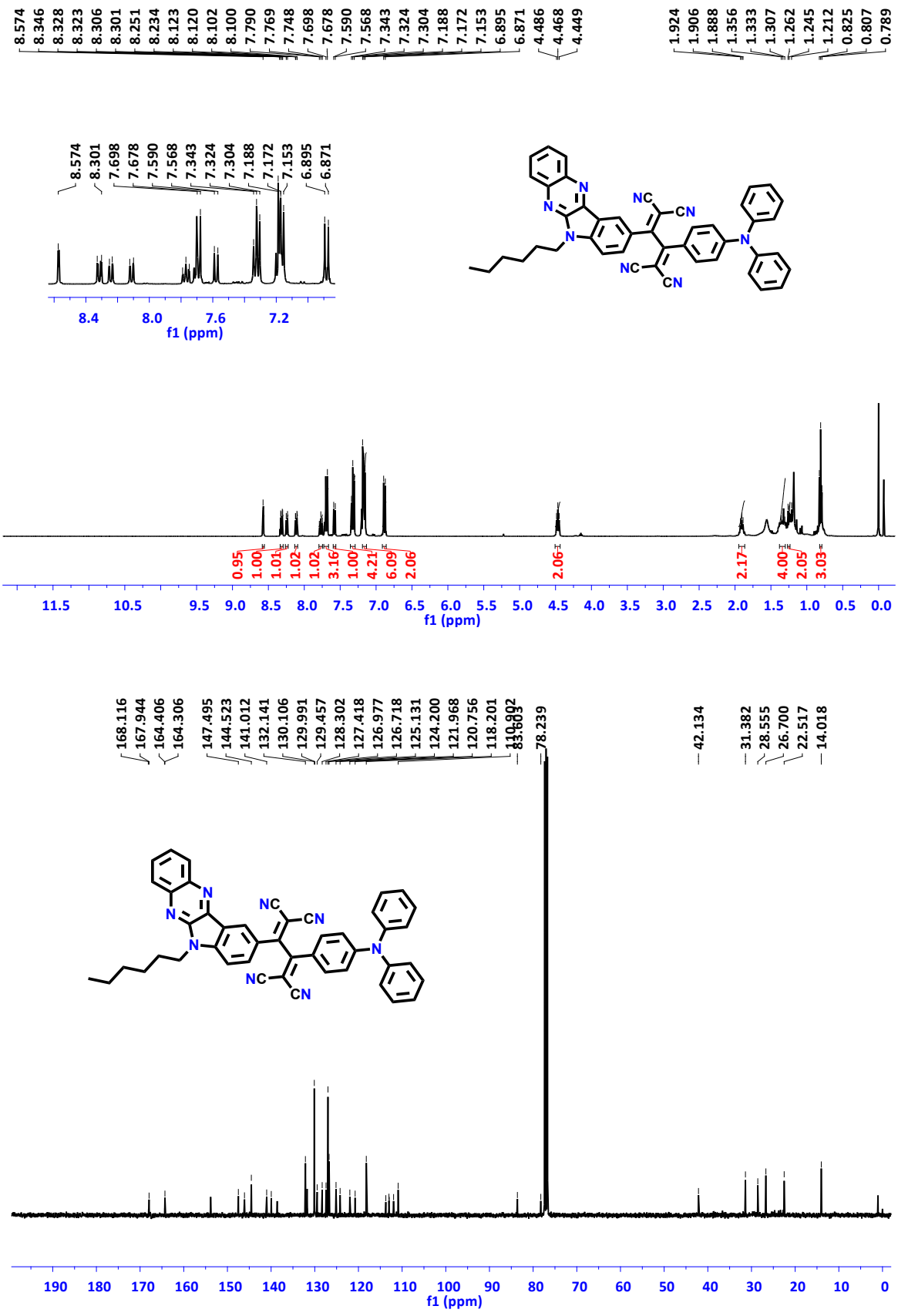

Figure S13: ^{1}H and ^{13}C NMR spectra of compound 10a

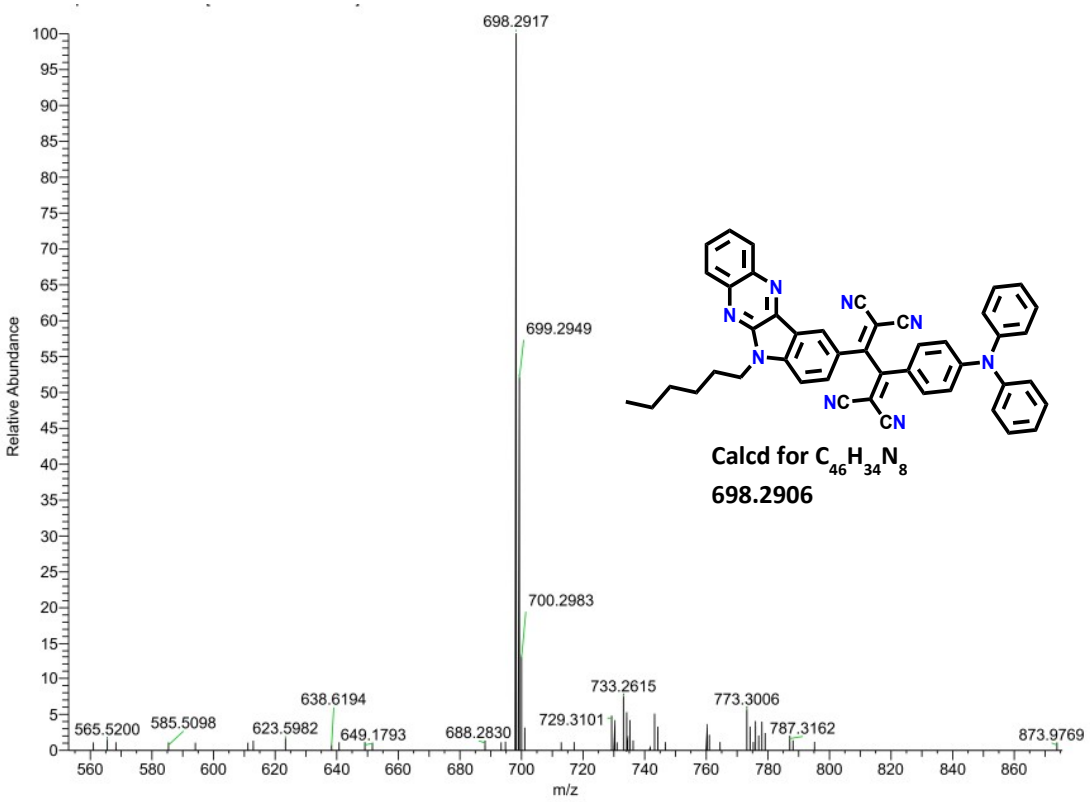

Figure S14: HRMS spectrum of compound 10a

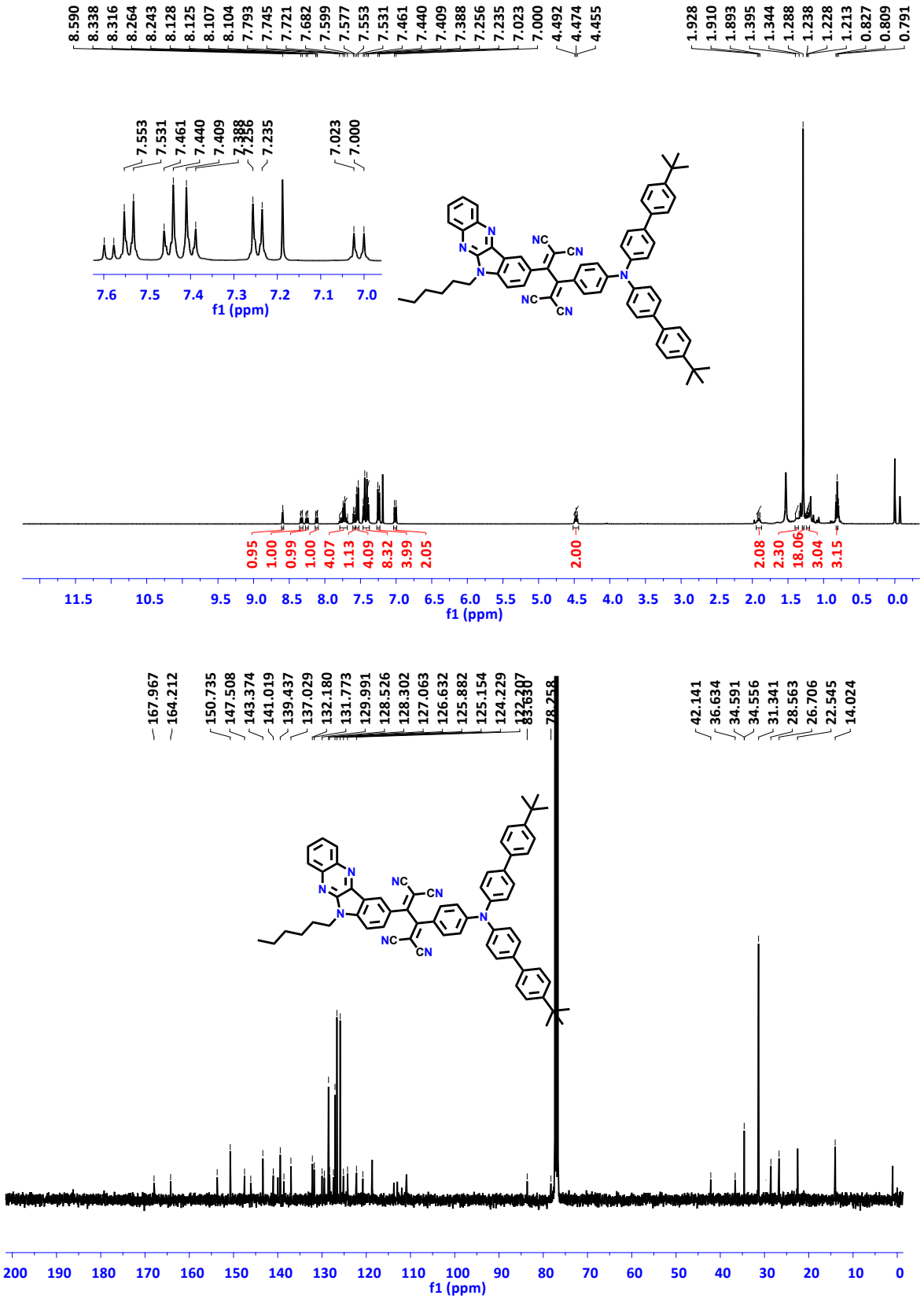

Figure S15: ^{1}H and ^{13}C NMR spectra of compound 10b

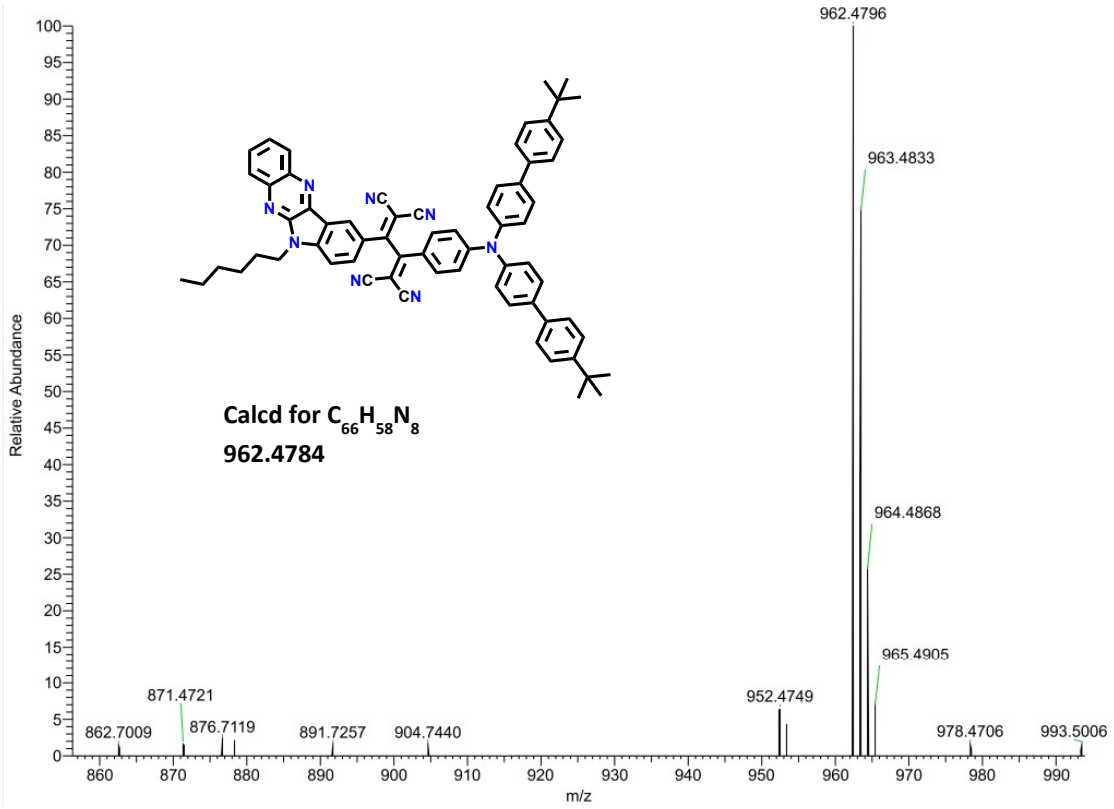

Figure S16: HRMS spectrum of compound 10b

3. Electrochemical characterizations of compounds 8a-b, 9a-b and 10a-b

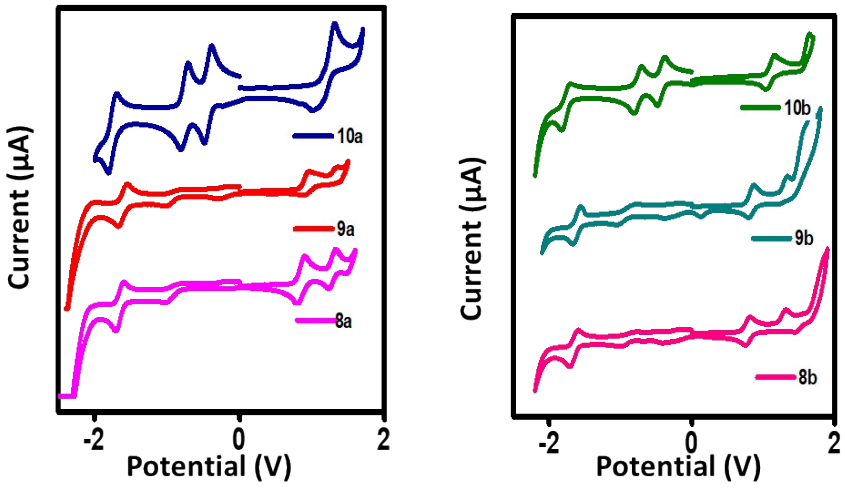

Figure S17: Cyclic voltammogram of compounds 8a-b, 9ab and 10a-b

4. XRD characterization of compounds 8a-b, 9ab and 10a-b

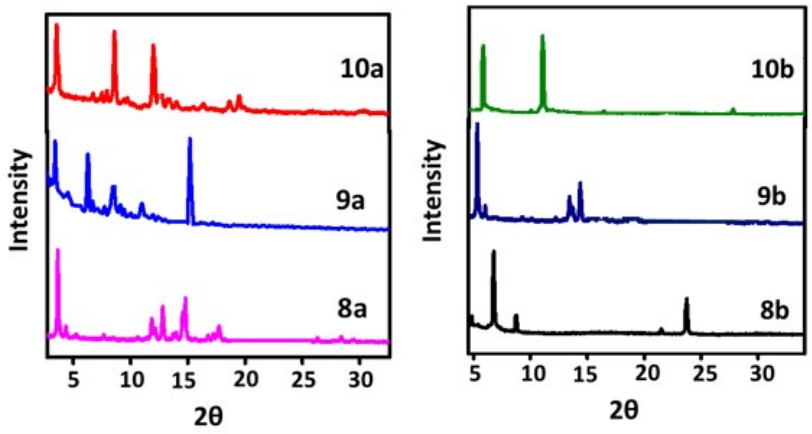

Figure S18: XRD of compounds 8a-b, 9ab and 10a-b

Two-dimensional grazing incidence X-ray diffraction measurements were performed to investigate the orientations and interchain packing in semiconductor films. The highest crystalline peaks observed for all the compounds support the long-range molecular ordering of the thin film.

5. Organic field-effect transistor: Device Fabrication

Organic field-effect transistors of **8a-b, 9a-b,** and **10a-b** were fabricated using bottom gate-top contact architecture over heavily doped n^{++} silicon. Silicon substrates were cleaned sequentially with heated acetone, methanol, and isopropanol for 15 mins and then rinsed with deionized water. Then, the Si wafers were cleaned by immersion in mild base piranha solution for 10 min, followed by rinsing with copious amounts of deionized water and drying in a flow of nitrogen. This procedure was repeated to reach the hydrophobicity on the Si wafer. Cleaned wafers were heated at 1200 °C for 90 mins to grow the SiO_2 layer, which serves as the gate dielectric. The thickness of the dielectric is ~300 nm. Compounds **8a-b, 9a-b,** and **10a-b** were dissolved in anhydrous chloroform at a concentration of 5 mg/mL, which was sonicated for 15 mins and filtered to get a homogenous solution. The active

layer was prepared by spin coating at 2000 rpm for 30 s in ambient conditions. Thus, prepared devices were annealed at 80 °C for 45. Finally, silver contacts were made for the source (S) and drain (D) electrodes with a channel length of 150 µm and width of 0.5 cm, and a silicon wafer acted as a gate. The capacitance of the dielectric layer is 8.3×10^{-9} F. Field-effect characteristics of the devices were analyzed in the air using a Keithley 4200A semiconductor parameter analyser.

OFET data of compound 8a

Table S1. Compound 8a OFET characteristics

8a Trials	μ_h cm^2/Vs			μ_e cm^2/Vs		
	µ	On/off ratio	V_{Th} (V)	µ	On/off ratio	V_{Th} (V)
1	0.43	10^6	-7	-	-	-
2	0.59	10^4	-20	-	-	-
3	0.43	10^5	-3	-	-	-
4	0.46	10^7	-5	-	-	-
5	0.45	10^5	-6	-	-	-
6	0.55	10^4	-10	-	-	-
7	0.45	10^4	-7	-	-	-
8	0.38	10^2	-2	-	-	-
9	0.40	10^5	-1	-	-	-
10	0.52	10^4	-7	-	-	-
11	0.62	10^4	-7	-	-	-
12	0.55	10^4	-15	-	-	-
13	0.42	10^5	-9	-	-	-
14	0.59	10^4	-15	-	-	-
15	0.62	10^5	-12	-	-	-

1

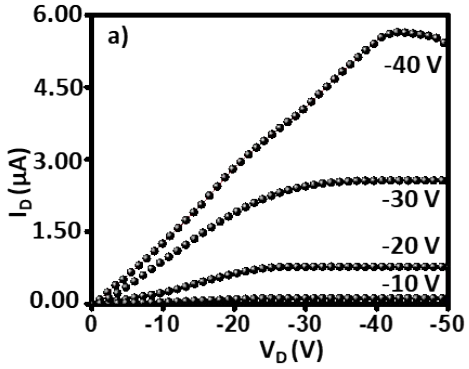
a)
-40 V
-30 V
-20 V
-10 V
I_D (μA)
V_D (V)

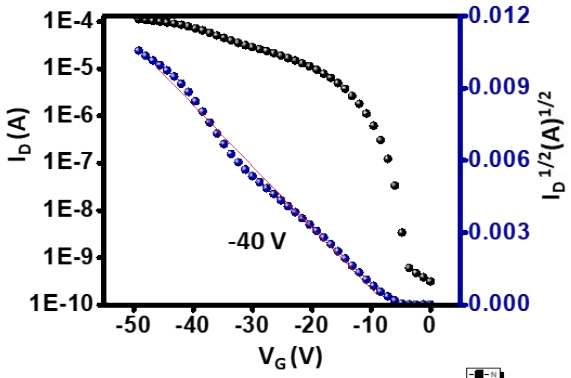
-40 V
I_D (A)
$I_D^{1/2}(A)^{1/2}$
V_G (V)

2

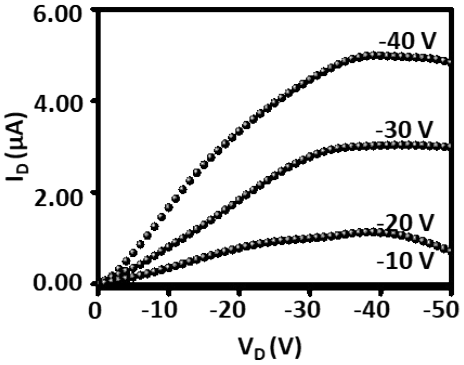
-40 V
-30 V
-20 V
-10 V
I_D (μA)
V_D (V)

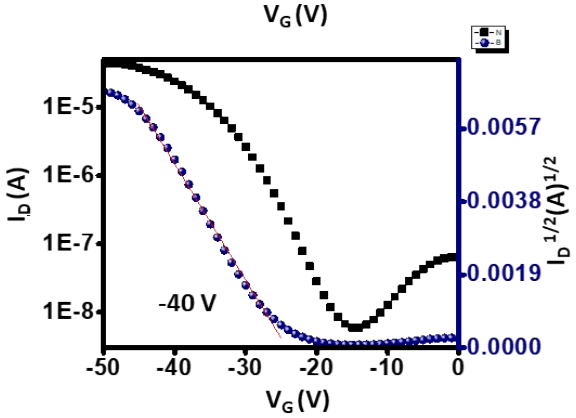
-40 V
I_D (A)
$I_D^{1/2}(A)^{1/2}$
V_G (V)

3

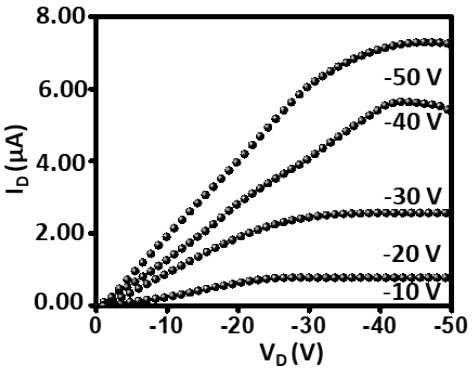
-50 V
-40 V
-30 V
-20 V
-10 V
I_D (μA)
V_D (V)

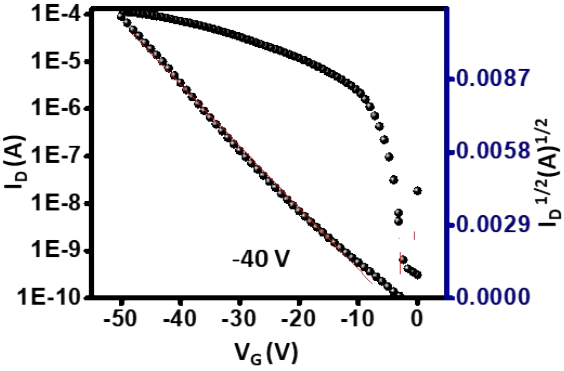
-40 V
I_D (A)
$I_D^{1/2}(A)^{1/2}$
V_G (V)

4

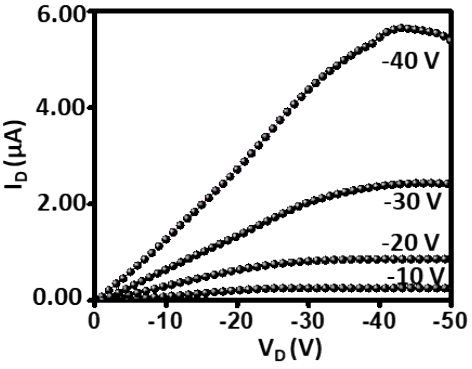
-40 V
-30 V
-20 V
-10 V
I_D (μA)
V_D (V)

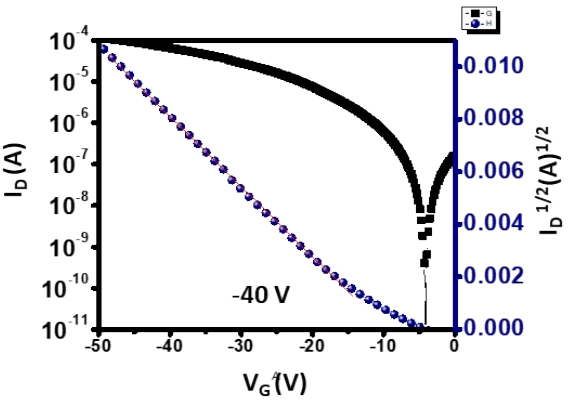
-40 V
I_D (A)
$I_D^{1/2}(A)^{1/2}$
V_G (V)

5

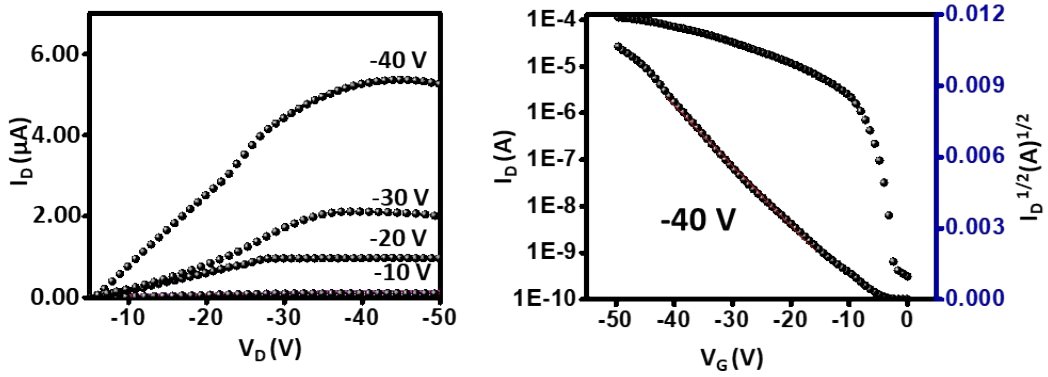
-40 V
-30 V
-20 V
-10 V
I_D (μA)
V_D (V)
-40 V
I_D (A)
$I_D^{1/2}(A)^{1/2}$
V_G (V)

6

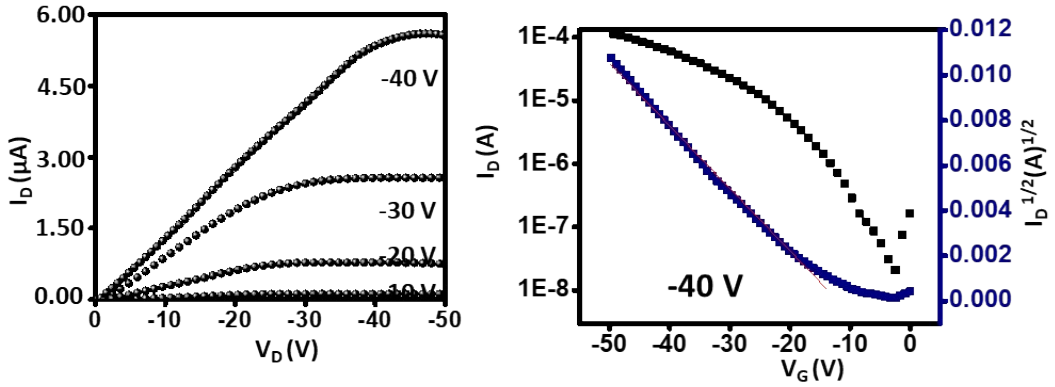
-40 V
-30 V
-20 V
I_D (μA)
V_D (V)
-40 V
I_D (A)
$I_D^{1/2}(A)^{1/2}$
V_G (V)

7

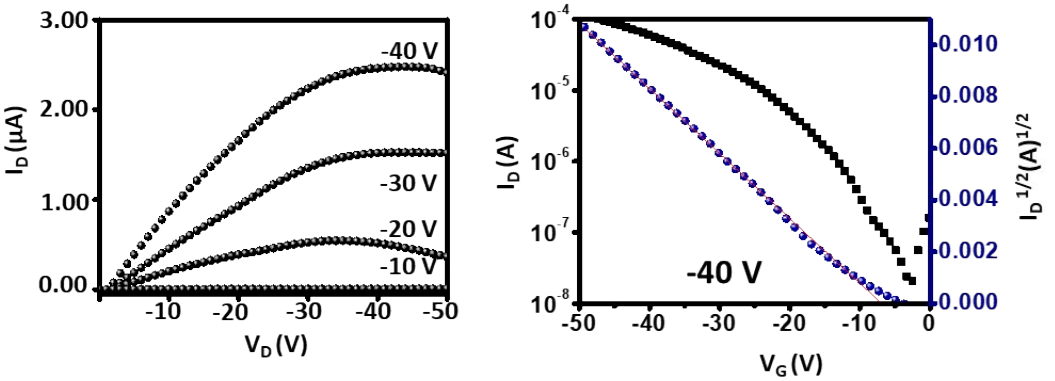
-40 V
-30 V
-20 V
-10 V
I_D (μA)
V_D (V)
-40 V
I_D (A)
$I_D^{1/2}(A)^{1/2}$
V_G (V)

8

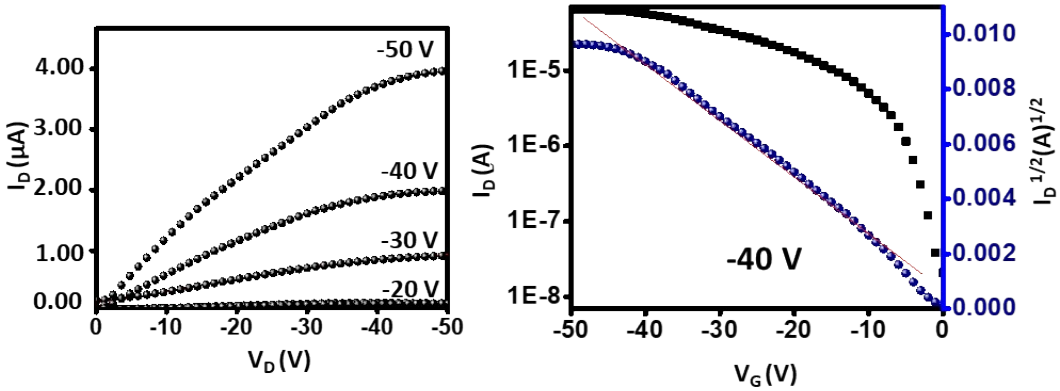
-50 V
-40 V
-30 V
-20 V
I_D (μA)
V_D (V)
-40 V
I_D (A)
$I_D^{1/2}(A)^{1/2}$
V_G (V)

9

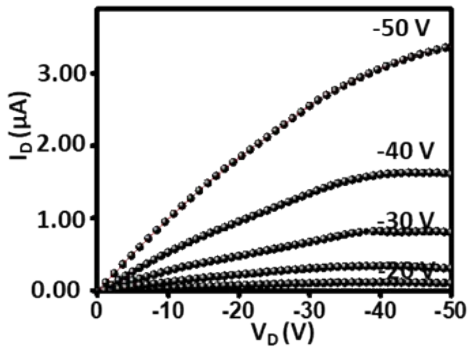
-50 V
-40 V
-30 V
-20 V
I_D (μA)
V_D (V)

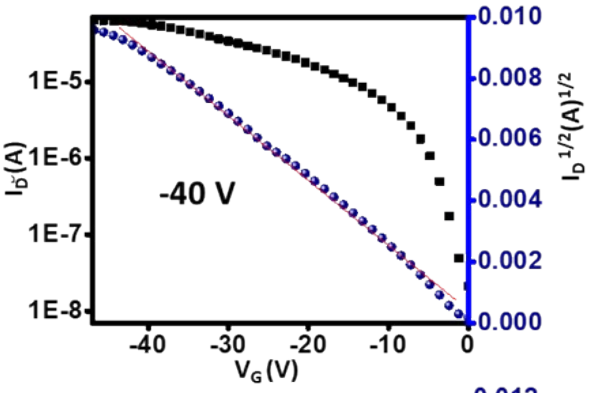
-40 V
I_D (A)
$I_D^{1/2}(A)^{1/2}$
V_G (V)

10

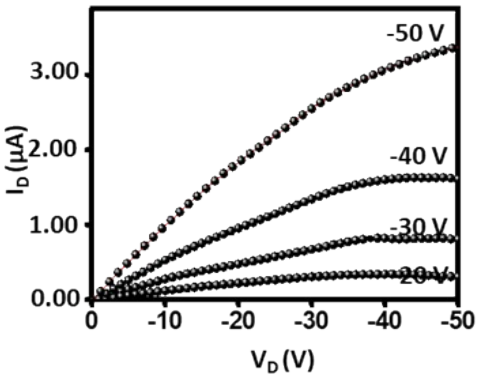
-50 V
-40 V
-30 V
-20 V
I_D (μA)
V_D (V)

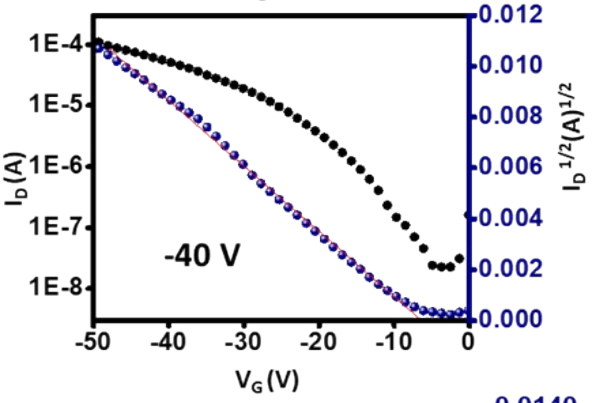
-40 V
I_D (A)
$I_D^{1/2}(A)^{1/2}$
V_G (V)

11

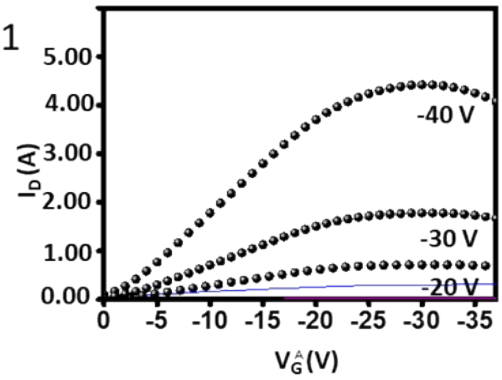
-40 V
-30 V
-20 V
I_D (A)
V_G (V)

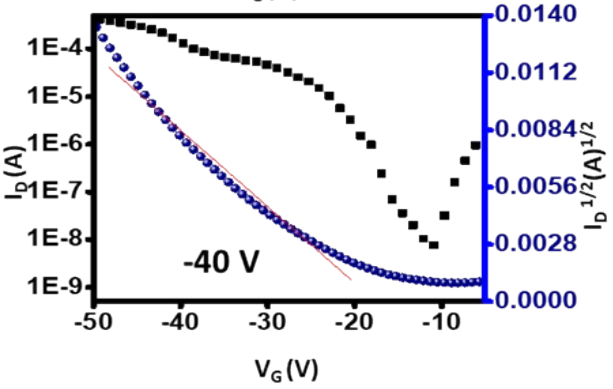
-40 V
I_D (A)
$I_D^{1/2}(A)^{1/2}$
V_G (V)

12

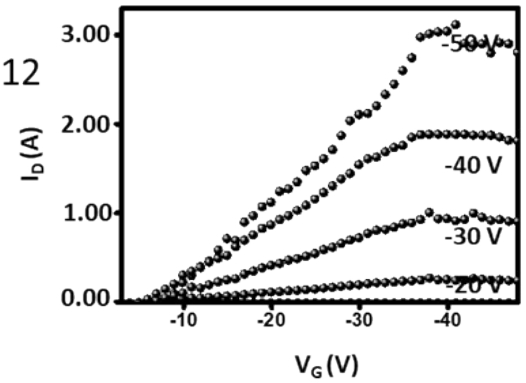
-40 V
-30 V
I_D (A)
V_G (V)

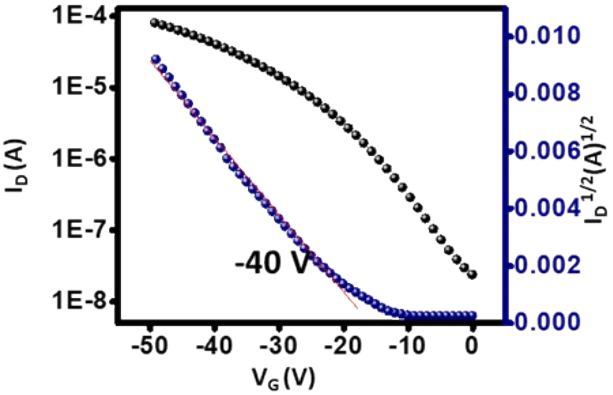
-40 V
I_D (A)
$I_D^{1/2}(A)^{1/2}$
V_G (V)

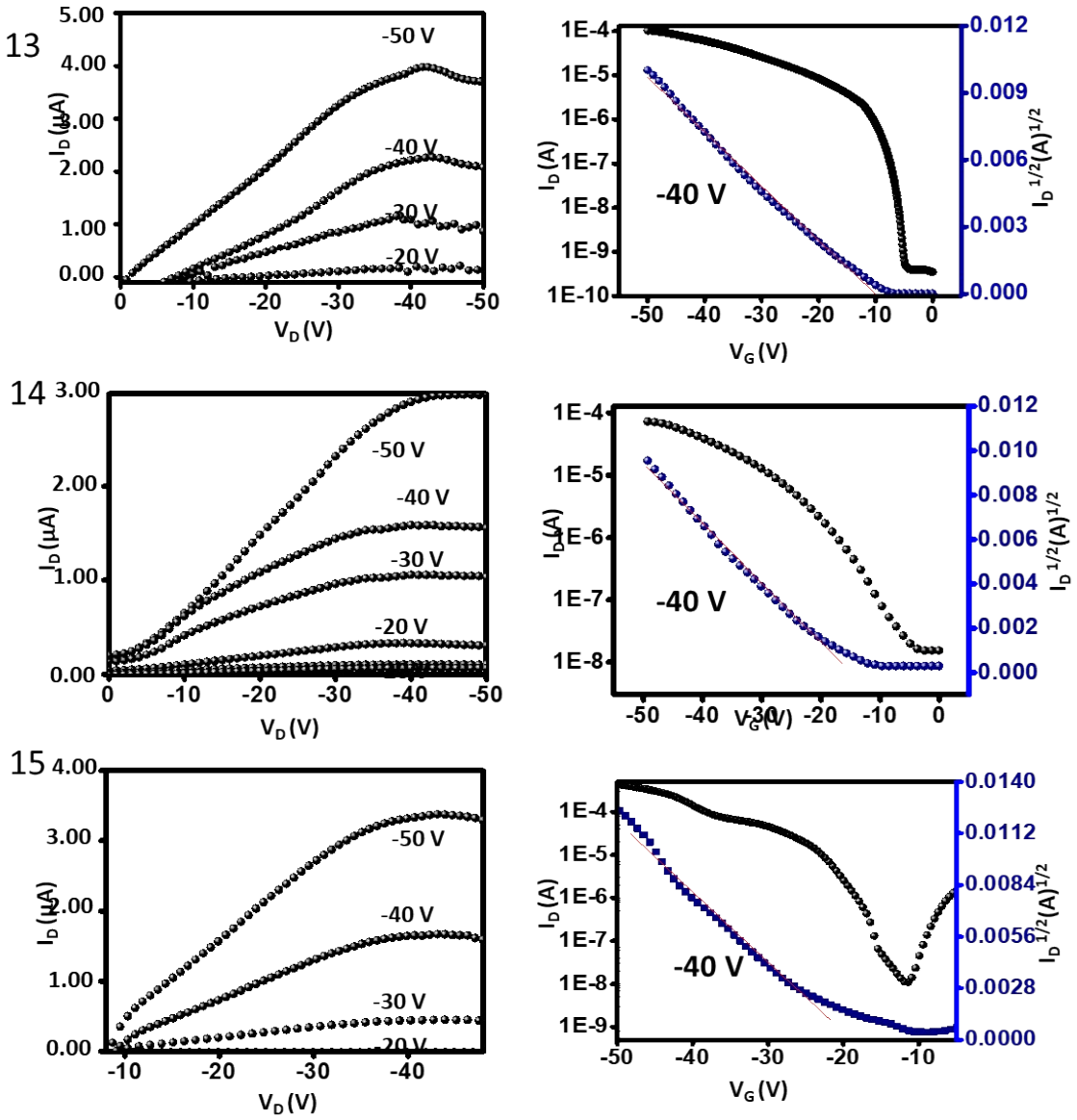

Figure S19: Trials of OFET devices of compound 8a

OFET data of compound 9a

Table S2. Compound 9a OFET characteristics

9a Trials	μ_h cm^2/Vs			μ_e cm^2/Vs		
	μ	On/off ratio	V_{Th} (V)	μ	On/off ratio	V_{Th} (V)
1	1.5	10^5	-10	-	-	-
2	0.7	10^5	-10	-	-	-
3	1.1	10^5	-20	-	-	-
4	1.1	10^5	-3	-	-	-
5	1.3	10^5	-5	-	-	-
6	1.2	10^5	-10	-	-	-
7	1.0	10^7	-5	-	-	-
8	1.1	10^4	-3	-	-	-
9	1.0	10^4	-1	-	-	-
10	1.1	10^5	-2	-	-	-
11	0.9	10^6	-2	-	-	-
12	1.3	10^6	-5	-	-	-
13	1.3	10^4	-7	-	-	-
14	1.2	10^5	-9	-	-	-
15	0.7	10^6	-10	-	-	-

OFET data of compound 10a

Table S3. Compound 10a OFET characteristics

8c Trials	μ_h cm^2/Vs			μ_e cm^2/Vs		
	μ	On/off ratio	V_{Th} (V)	μ	On/off ratio	V_{Th} (V)
1	0.32	10^6	-20	0.9	10^5	19
2	0.30	10^6	-20	1.6	10^5	20
3	0.20	10^5	-21	0.2	10^2	15
4	0.20	10^4	-15	0.3	10^5	13
5	0.09	10^4	-20	1.2	10^4	12
6	0.10	10^4	-10	1.3	10^4	17
7	0.10	10^3	-15	1.2	10^5	20
8	0.32	10^4	-10	1.7	10^2	20
9	0.28	10^4	-15	0.4	10^3	10
10	0.25	10^5	-20	0.6	10^4	5
11	0.20	10^4	-5	0.5	10^4	7
12	0.20	10^4	-5	0.4	10^2	9
13	0.10	10^4	-10	1.2	10^4	11
14	0.10	10^4	-5	1.3	10^5	13
15	0.21	10^5	-7	1.1	10^4	15

OFET data of compound 8b

Table S4. Compound 8b OFET characteristics

8b Trials	μ_h cm^2/Vs			μ_e cm^2/Vs		
	μ	On/off ratio	V_{Th} (V)	μ	On/off ratio	V_{Th} (V)
1	0.64	10^6	-12	-	-	-
2	0.63	10^6	-12	-	-	-
3	0.60	10^5	-10	-	-	-
4	0.50	10^6	-10	-	-	-
5	0.60	10^5	-12	-	-	-
6	0.40	10^4	-15	-	-	-
7	0.40	10^4	-20	-	-	-
8	0.55	10^5	-7	-	-	-
9	0.45	10^5	-9	-	-	-
10	0.60	10^6	-10	-	-	-
11	0.55	10^5	-7	-	-	-
12	0.50	10^6	-10	-	-	-
13	0.50	10^4	-12	-	-	-
14	0.45	10^5	-9	-	-	-
15	0.45	10^5	-5	-	-	-

OFET data of compound 9b

Table S5. Compound 9b OFET characteristics

9b Trials	μ_h cm^2/Vs			μ_e cm^2/Vs		
	μ	On/off ratio	V_{Th} (V)	μ	On/off ratio	V_{Th} (V)
1	1.1	10^6	-20	-	-	-
2	1.25	10^6	-21	-	-	-
3	1.05	10^5	-15	-	-	-
4	1.20	10^6	-20	-	-	-
5	1.2	10^5	-15	-	-	-
6	1.0	10^3	-10	-	-	-
7	1.1	10^4	-14	-	-	-
8	0.9	10^5	-20	-	-	-
9	1.05	10^5	-15	-	-	-
10	1.21	10^6	-20	-	-	-
11	1.10	10^5	-19	-	-	-
12	1.20	10^6	-20	-	-	-
13	0.95	10^4	-15	-	-	-
14	1.20	10^5	-10	-	-	-
15	0.95	10^5	-7	-	-	-

OFET data of compound 10b

Table S6. Compound 10b OFET characteristics

10b Trials	μ_h cm^2/Vs			μ_e cm^2/Vs		
	μ	On/off ratio	V_{Th} (V)	μ	On/off ratio	V_{Th} (V)
1	0.35	10^5	-20	2.1	10^6	22
2	0.25	10^5	-25	1.2	10^6	20
3	0.30	10^6	-15	0.4	10^3	21
4	0.25	10^6	-20	0.5	10^3	20
5	0.30	10^5	-15	0.6	10^3	19
6	0.32	10^5	-10	0.9	10^6	18
7	0.25	10^5	-14	2.0	10^6	15
8	0.30	10^4	-20	1.8	10^6	10
9	0.32	10^4	-15	1.9	10^6	13
10	0.33	10^5	-20	1.5	10^6	15
11	0.25	10^5	-18	1.5	10^5	20
12	0.26	10^6	-19	0.8	10^5	21
13	0.30	10^5	-20	0.9	10^6	20
14	0.35	10^5	-22	0.9	10^6	15
15	0.25	10^4	-20	0.8	10^4	10

6. Computational Studies of compounds 8a-b, 9a-b, and 10a-b:

A series of computational simulations, such as molecular mechanics and semi-empirical methods, were used for packing and predicting the electronic properties of the system. The approximate geometrical parameters were used to compute the optimized structure at the DFT's B3LYP level of theory and TD-SCF for spectral estimation.[1-2] The DFT calculations were performed with the Gaussian at the 6-31D level of theory. All the molecules were optimized by considering symmetry in effect. MedA was used to calculate the bandgap, and the FMOs were visualized using *Gaussview software.*

The optimized geometry was used as input for Density of States (DOS) calculations using VASP (MedeA, Materials Design, http://www.materialsdesign.com) software. The structures were evaluated involving solvent correction parameter GGA-PBE basis set.

The crystallographic values were obtained from the VASP software, and the crystal parameters and setup packing pattern were assigned using *Discovery Studio* Software. The packing patterns were modeled with various group symmetry elements, and only those given plausible parameters were considered for computing hopping values.

To understand the origin of unique spectroscopic properties time dependent-SCF calculations were performed on those molecules. The optical bands of these compounds arise from the combinations of multiple HOMO-*n*→LUMO+*m* transitions, which are quite in agreement with experimental results. The oscillator strength, transition energies, and the most relevant singlet excited state assignments are given in **Table S1**. The lowest energy transition of the compounds above 400-500 nm corresponds to the charge transfer from HOMO to LUMO. The band around 350 nm is attributed to the multiple overlaps of π-π* transitions involving HOMO-1 and LUMO+1 orbitals.[3]

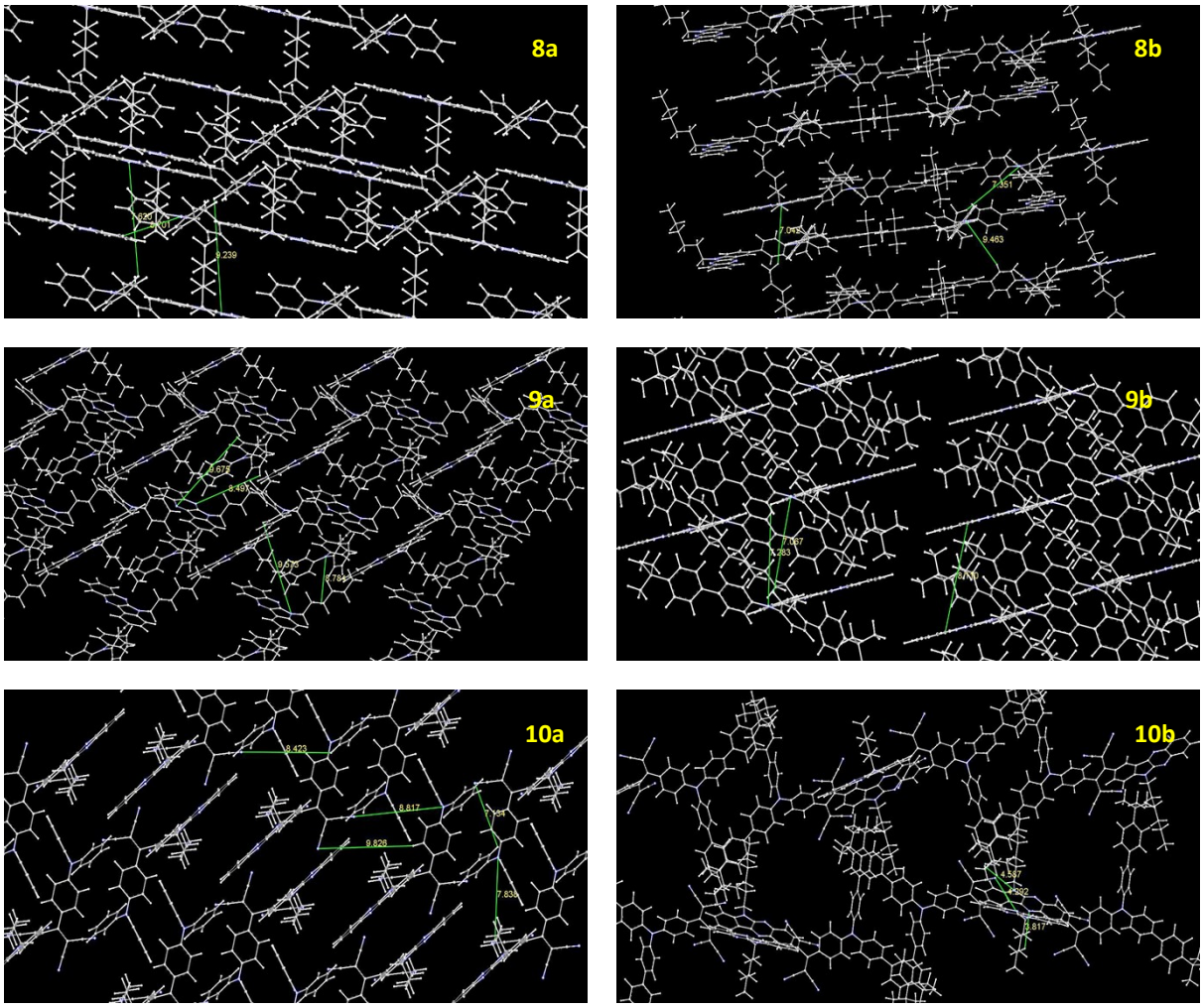

Figure S20: Crystalline packing of compounds 8a-b, 9a-b and 10a-b

Table S7: Electronic absorption behaviour of compounds 8a-b, 9a-b and 10a-b

	Wavelength nm	Energy eV	Oscillator Strength F	Type of transition
8a	474.2	2.614	0.012	S_0-S_1
	445.2	2.785	0.021	S_{-1}-S_1
	384.9	3.221	0.027	S_{-1}-S_1
	342.6	3.619	0.007	S_{-4}-S_1
8b	454.5	2.728	0.027	S_{-1}-S_1
	488.2	2.539	0.011	S_0-S_1
	393.1	3.154	0.035	S_{-1}-S_1
	363.5	3.410	1.072	S_0-S_2
9a	435.3	2.848	0.027	S_{-1}-S_1
	388.8	3.188	1.451	S_0-S_2
	461.5	2.686	0.000	S_{-3}-S_1
	377.0	3.288	1.543	S_0-S_2
9b	94.4	3.146	1.587	S_0-S_2
	439.4	2.822	0.066	S_{-1}-S_1
	399.4	3.144	1.546	S_0-S_2
	468.2	2.647	0.000	S_{-4}-S_1
10a	554.4	2.236	0.183	S_0-S_1
	494.3	2.508	0.116	S_{-1}-S_1
	476.6	2.601	0.125	S_{-1}-S_1
	429.9	2.884	0.526	S_0-S_2
10b	521.9	2.375	0.000	S_0-S_2
	477.7	2.595	0.045	S_0-S_2
	459.5	2.698	0.487	S_0-S_2
	508.5	2.438	0.147	S_{-1}-S_1

Crystal parameters were predicted by MedeA packing pattern, and the intermolecular distances between the molecular systems were calculated considering non-covalent interactions. The space groups were chosen to represent the plausible crystalline structure, the possible packing is illustrated in **Figure S19,** and the parameters are given in **Table S2**. All the molecules showed good crystalline packing due to the planar configuration of the planar indoloquinoxaline moiety. Compound **8a** exhibited an orthorhombic pattern appearing triphenylamine part of one molecule is exactly opposite to the indoloquinoxaline unit of another molecule. Besides, compound **8b** has a packing pattern quite similar to the **9a** with little lowered intermolecular interactions of 7.042 Å. The ethynyl bridge present in the molecules assists in a favorable stacking arrangement.

The substitution of the tetracyanoethylene group in between the indoloquinoxaline and triphenylamine in compounds **10a-b**, significantly affects crystalline properties. The molecule shows non-covalent interactions with the intermolecular distance of 3.817 Å for **10b**; such low intermolecular distance supports the charge transport property of the compounds. Also, the compounds show CH-π interactions with a distance of 4.292 Å.

Table S8: **Crystal structure and lattice parameters of *8a-b, 9a-b and 10a-b***

	Cell Parameters a / b / c α / β / γ	Type of Cell	Preferences	Symmetry	Intermolecular Distances Å
8a	22.3/17.4/8.24 90/90/90	simple orthorhombic	331	P-1	7.620 8.701 9.239
8b	26.5/25.2/11.3 90/90/90	simple orthorhombic	115	P21/C	7.042 7.351 9.463
9a	22.4/17.2/9.3 90/90/90	simple orthorhombic	341	P2	8.497 8.784 9.573
9b	27.4/25.5/8.11 90/90/90	simple orthorhombic	123	P-1	7.067 7.283 8.110
10a	25.3/15.8/12.6 90/90/90	simple orthorhombic	214	P-1	7.134 7.836 8.817
10b	30.1/24.3/15.9 90/90/90	simple orthorhombic	113	P212121	3.817 4.292 4.587

The DOS states were utilized to calculate the number of available states in the systems, which can be used as a basis for the transport model.[16] The DOS diagrams of compounds **8a-b, 9a-b,** and **10a-b** are given in **Figure S20,** and the data are summarized in **Table S3**. The highest density of states was available for **8b** and **9b**, whereas it was relatively low for other compounds. The obtained closer Fermi levels to HOMO for these compounds facilitate the *p*-channel characteristics.

Table S9: DOS parameters of compounds 8a-b, 9a-b and 10a-b

	Molecular Formula	Free Energy (eV)	Density (mg/m^3)	DOS Gap (eV)	Band gap (eV)	E Fermi (eV)
8a	$C_{38}\ N_4\ H_{34}$	-501.19	0.504	2.8599	2.254	-3.3997
8b	$C_{58}\ N_4\ H_{58}$	-771.06	0.354	3.2545	1.728	-3.5901
9a	$C_{40}\ N_4\ H_{34}$	-517.51	0.470	3.0262	2.209	-3.4689
9b	$C_{60}\ N_4\ H_{58}$	-787.36	0.436	2.2745	2.082	-3.4407
10a	$C_{46}\ N_8\ H_{34}$	-601.63	0.456	1.3320	1.225	-4.2724
10b	$C_{66}\ N_8\ H_{58}$	-871.65	0.272	1.2260	1.323	-4.4978

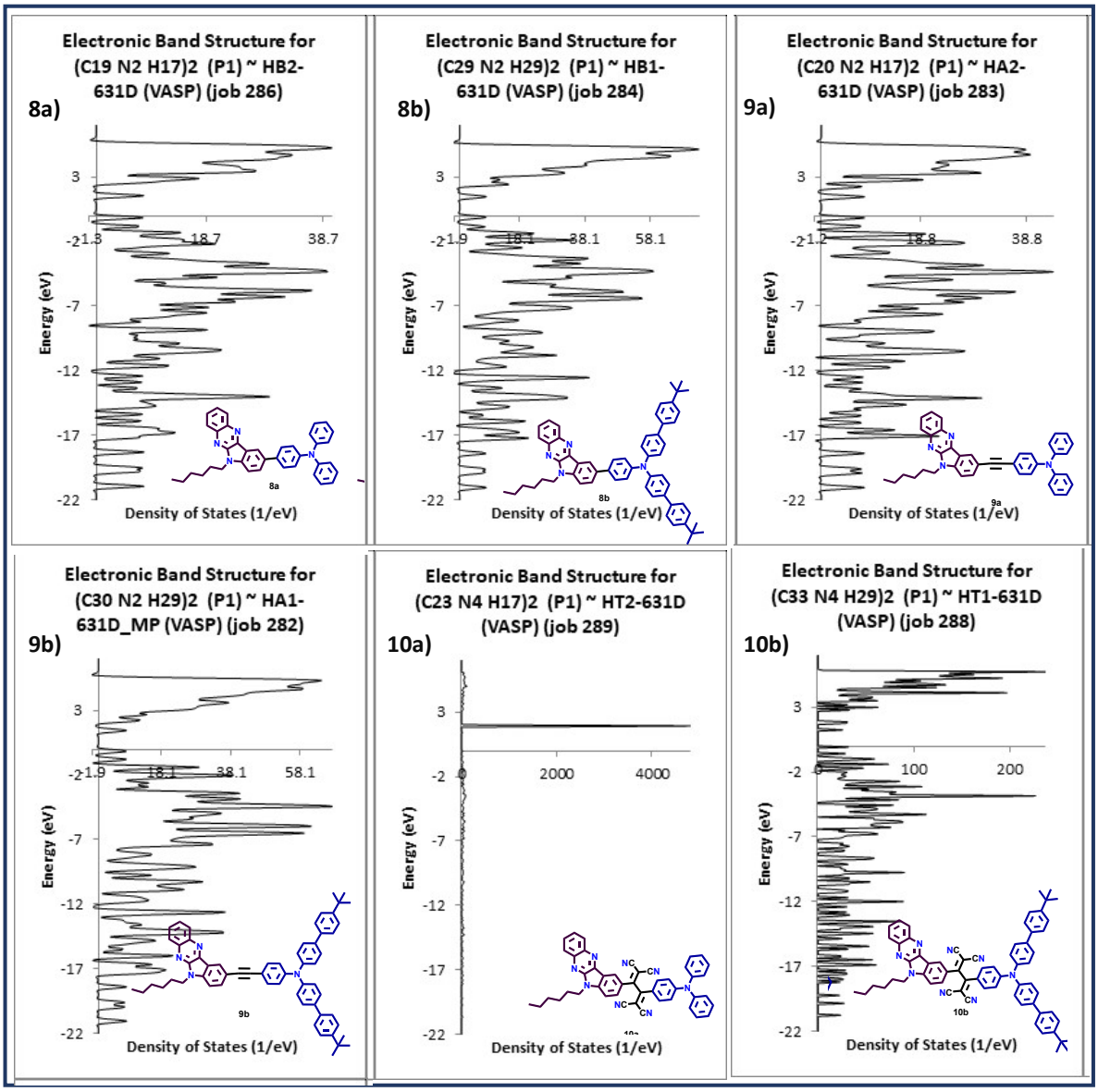

Figure S21: DOS diagram of compounds 8a-b, 9a-b and 10a-b

References:

(1) Bracker, M.; Dinkelbach, F.; Weingart, O.; Kleinschmidt, M. Impact of Fluorination on the Photophysics of the Flavin Chromophore: A Quantum Chemical Perspective. *Phys. Chem. Chem. Phys.* **2019**, *21* (19), 9912–9923.

(2) Huang, C.; Zhen, C.-G.; Su, S. P.; Loh, K. P.; Chen, Z.-K. Solution-Processable Polyphenylphenyl Dendron Bearing Molecules for Highly Efficient Blue Light-Emitting Diodes. *Org. Lett.* **2005**, *7* (3), 391–394. https://doi.org/10.1021/ol0478180.

(3) Frisch, M. J.; Trucks, G. W.; Schlegel, H. B.; Scuseria, G. E.; Robb, M. A.; Cheeseman, J. R.; Scalmani, G.; Barone, V.; Mennucci, B.; Petersson, G. A.; Nakatsuji, H.; Caricato, M.; Li, X.; Hratchian, H. P.; Izmaylov, A. F.; Bloino, J.; Zheng, G.; Sonnenberg, J. L.; Hada, M.; Ehara, M.; Toyota, K.; Fukuda, R.; Hasegawa, J.; Ishida, M.; Nakajima, T.; Honda, Y.; Kitao, O.; Nakai, H.; Vreven, T.; Montgomery, J. A.; Peralta, J. E.; Ogliaro, F.; Bearpark, M.; Heyd, J. J.; Brothers, E.; Kudin, K. N.; Staroverov, V. N.; Kobayashi, R.; Normand, J.; Raghavachari, K.; Rendell, A.; Burant, J. C.; Iyengar, S. S.; Tomasi, J.; Cossi, M.; Rega, N.; Millam, N. J.; Klene, M.; Knox, J. E.; Cross, J. B.; Bakken, V.; Adamo, C.; Jaramillo, J.; Gomperts, R.; Stratmann, R. E.; Yazyev, O.; Austin, A. J.; Cammi, R.; Pomelli, C.; Ochterski, J. W.; Martin, R. L.; Morokuma, K.; Zakrzewski, V. G.; Voth, G. A.; Salvador, P.; Dannenberg, J. J.; Dapprich, S.; Daniels, A. D.; Farkas, O.; Foresman, J. B.; Ortiz, J. V.; Cioslowski, J.; Fox, D. J.. Gaussian 09, revision A.1; Gaussian, Inc.: Wallingford, CT, 200